Development of a Correlation to Correct Mercury Intrusion Porosimetry Data

By

Abiashue Lucky

A Thesis submitted to the School of Graduate Studies in partial fulfillment of the requirements for the degree of

Master of Engineering

Faculty of Engineering and Applied Science

Memorial University of Newfoundland

October, 2023

St John's, Newfoundland and Labrador, Canada.

Abstract

Analysis of the core data, such as capillary pressure, permeability, and porosity is important in assessing and modeling hydrocarbon flow in a reservoir. Mercury intrusion porosimetry (MIP) method is the fastest and least expensive method of measuring capillary pressure compared to other methods such as centrifuge, porous plate, and vapor desorption. In addition to the injection pressure versus mercury saturation, this method also provides porosity and pore size distribution of the sample. The sample permeability can then be estimated using models with parameters such as capillary pressure, mercury saturation and others. Previous research shows that MICP tests generate saturations curves that are lower than those obtained from other methods. The aim of this work is to improve on the permeability and porosity results obtained using mercury intrusion porosimetry method by comparing them against more accurate measurements such as gas permeametry and porosimetry, and finally develop a correlation based on which the data from mercury porosimetry tests could be corrected. The literature review conducted as a part of this study confirmed that such a correction has not been proposed in the literature.

In this research work, MIP method was used to measure porosity and permeability of Nineteen core plug samples from HIBERNIA B16-17, a well drilled offshore Newfoundland and Labrador (Canada). For comparison purposes, the same samples were used for permeability measurement using a more accurate method known as Klinkenberg-corrected gas permeametry. For porosity comparison, some helium pycnometry data were found in the literature for samples collected from the same reservoir / reservoir depth as those of the core plug samples used in this study. In addition, a well-accepted correlation from the literature, known as Swanson model, was used to calculate core plug permeabilities for comparison against measurements. These comparative analyses resulted in improved understanding about the trends and provided correlations between the

measurement methods. The resulting correlations can be used to correct the porosity and permeability values obtained from the MIP method and improve accuracy. The comparative analysis conducted in this study shows that the porosity values obtained by helium pycnometry are mostly greater than those obtained by the MIP method with an average difference of 9.8%. In addition, the permeability values obtained from the Klinkenberg-corrected gas permeametry are greater than the results from the MIP method with an average difference of 22.9%. The permeability data estimated by Swanson correlation exhibited higher error when compared to the gas permeametry data, with an average percentage difference of 49.3%. Both the porosity and permeability values obtained from the MIP method are generally lower than the more accurate data collected from gas porosimetry or permeametry; therefore, applying the proposed correction is recommended to generate more accurate porosity and permeability values.

Acknowledgements

I would like to express my gratitude to my supervisor, Dr. Lesley James, who supported me throughout the course of my studies at Memorial University. Without her support and persistent help, it would have not been possible to complete this dissertation.

I would like to thank the support and help provided by the Faculty of Engineering and Applied Science staff, Norah Hyndman, Dr. Omidreza Mohammadzadeh, Edison Sripal, and Maziyar Mamoodi for their assistance with lab setup and review of the thesis.

Finally, I would like to dedicate this work to my wife Susan and my family for their support, encouragement, understanding and companionship during the course of my studies, and to all my friends, who are too numerous to mention.

Table of Contents

List of Figures

List of Tables

List of Abbreviations

A Area

a Constants for Swanson model

a_0 Model parameters in Liu et al. (2016) permeability model

a_1 Model parameters in Liu et al. (2016) permeability model

B_∞ Percent bulk volume occupied by mercury at infinite capillary pressure

BPR Back pressure regulator

B_v Volume fraction

c Constant for Swanson model

C Constant in modified Swanson model

cc Centimeter cube

D Model parameters in Liu et al. (2016) permeability model

DP Pressure Difference

DVS Dynamic vapor sorption

F Lithology factor

G Pore geometrical factor

HPHT High pressure high temperature

IFT Interfacial tension

k Permeability

L Length of the sample

Md	Millidarcy
MICP	Mercury Intrusion Capillary Pressure
MIP	Mercury intrusion Porosimetry
MP	Mercury Porosimerty
n.d	No date
nD	Nanodarcy
mD	Milidarcy
nm	Nanometer
P_1	Inlet Pressure
P_2	Outlet Pressure
P_c	Capillary pressure
P_d	Extrapolated displacement pressure
P_m	Mean Pressure
r	Pore throat size radius
S_b	Percent bulk volume occupied by mercury
STO	Stock tank oil
T	Surface tension
Vp	Pore volume
Vs	Volume of solids
μ	Viscosity

μm	Micrometer
ϕ	Porosity
P	Average capillary pressure value for the effective pore throat diameter
σ	Interfacial tension
θ	Contact angle
γ σ, T	Surface tension
Q	Flowrate
Atm	Amospheric pressure
Temp	Temperature
Dia	Diameter
Abs	Absolute
Cc/min	Cubic centimeter per minute
ST DEV	Standard deviation
COV	Coefficient of variation
B&A	Bland-AlHtman
PT	Pressure Transducer
MPa	Megapascal
K_g	Gas Permeability
K_l	Liquid Permeability
°	Degrees

°C	Degree Centigrade
3D	Three Dimensional
a	Pore radius

Chapter 1: Introduction

1.1. Background

Data obtained from core analysis, including capillary pressure, permeability, and porosity is vital to assess and model reservoir-scale hydrocarbon flow. Hence, the accuracy of these data and the ease with which they are obtained are crucial. Mercury intrusion porosimetry (MIP) method is a faster and cheaper method to analyze capillary pressure compared to centrifuge, porous plate, vapor desorption or coreflooding methods [Al-Bulushi et al., 2019]. From the MIP test, very valuable rock properties are obtained such as porosity, injection pressure versus mercury saturation, and pore throat size distribution. The capillary pressure and pore throat size distribution can then be corelated to estimate the sample permeability. However, the MIP measurements are subject to some errors which make the data less accurate compared to other methods such as gas permeametry (for permeability measurement) or helium pycnometry (for porosity measurement). These errors arise from various sources such as sample size and shape, operating condition, mercury and penetrometer properties, core property measurement and conversion parameters [Nabil et al., 2019]. The permeability results derived from the MIP method are generally estimated and lower than the Klinkenberg-corrected permeability data, obtained from gas permeametry [Saki et al., 2020]. Therefore, a correction needs to be developed to relate the permeability data obtained from these two methods. This is also the case when it comes to comparing porosity data from the MIP method to the values obtained from gas pycnometry. The porosity values from MIP method are generally smaller than those from gas pycnometry method [Mastalerz et al., 2013]. Such a comparative study has not been done in the literature.

The objective of this research is to find a correction correlation for permeability and porosity results obtained from the MIP method by comparing the results with permeability and porosity values obtained from gas permeametry and helium pycnometry methods, respectively. The correction(s) can then be applied to future MIP measurements, resulting in better accuracy from a faster and cheaper porosity and permeability measurement method. The structure of this thesis is as follows: In Chapter Two, the fundamentals of core analysis are outlined. The relevant literature is reviewed in Chapter Three. The methodology of this research study is outlined in Chapter Four. The results are presented in Chapter Five, followed by discussion of results, conclusions and recommendations presented in Chapter Six.

Chapter 2: Fundamentals of Core Analysis

Cores are columnar rock samples usually taken from a borehole drilled in a target reservoir. The core samples are analyzed to characterize the reservoir rock. The test data helps in estimation of reservoir volume, formulation of development plans, as well as future production projection. Knowledge of the reservoir characteristics improves the success rate of oil and gas well development. Various rock and fluid properties are measured during the course of core analysis including porosity, permeability, electrical rock properties, capillary pressure, pore size distribution, relative permeability, to name a few.

2.1 Porosity

"Porosity is expressed as the percentage of the total bulk volume occupied by interstices" [API, 1941]. It expresses how porous the rock is; hence, it dictates the rock capacity for storing fluids. Porosity is mathematically defined as:

$$\emptyset = V - \frac{Vs}{V} = \frac{Vp}{V} = \frac{pore\ volume}{Total\ Bulk\ Volume} \qquad \text{Eq 2.1}$$

where "volume of solids" is denoted by *Vs, "total bulk volume"* is denoted by *V* and "pore volume" is given as $Vp = V - Vs$.

Porosity can be presented either as a fraction or percentage. It should be noted that porosity does not give any information concerning pore sizes, their distribution, or their degree of connectivity. Thus, rocks of the same porosity can have widely different physical properties. For instance, porosity of a carbonate core plug could be the same as that of a sandstone core plug; however, the carbonate porous system is in general less connected and therefore has smaller permeability value compared to that of the sandstone pore structure. There are various types of porosity defined for a particular porous medium [Paul, 2015]. From the origin point of view, porosity is divided to intergranular (primary), microporosity, dissolution (secondary), and fracture

for sandstone porous systems [Pittman, 1979]. For a carbonate porous system, however, the classification is much broader, and can be categorized into seven porosity types, namely interparticle, intraparticle, intercrystal, moldic, fenestral, fracture and vugs [Choquette and Pray, 1970]. From pore connectivity perspective, porosity is divided into two types: total porosity and effective porosity [Paul, 2015].

2.1.1 Porosity Measurement Methods

There are various porosity measurement methods in which different working fluids are used. Porosity can also be measured with no fluid involvement (i.e., image analysis method) or can be calculated using geometrical method. In this section, different porosity measurement methods are discussed:

2.1.1.1 Mercury intrusion porosimetry (MIP)

In this test, the porous sample is placed in a penetrometer, and a two-step pressurizing procedure is applied. First, a pressure of less than 30 psi is applied, and it is then increased to a final pressure of as high as 60,000 psi. Other information can also be determined using MIP method such as bulk and skeletal densities of the porous sample.

Upon increasing the mercury intrusion pressure, the intruded mercury volume is recorded at each pressure step. It is advised to obtain up to 100 pressure steps, but this depends on the nature of the sample as well as sample size, shape, and permeability [Leon, 1998]. In Figure1, various components used in the MIP setup are shown including penetrometer bulb and stem, as well as cap seal and component. The cap component holds the weighted porous sample (i.e., core plug or unconsolidated sample) in place during the analysis.

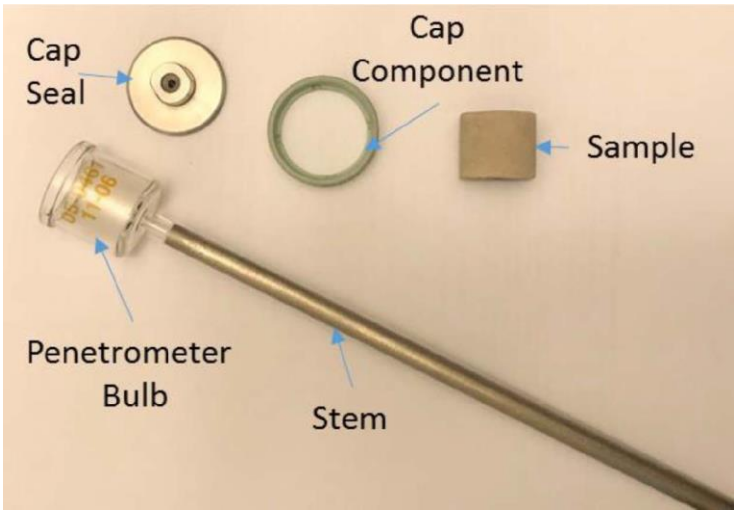

Figure 2.1:Penetrometer bulb and stem with the cap component [Al-Bulushi et al., 2019]

A schematic diagram describing different steps of the MIP test is presented in Figure 2. The system is evacuated first, followed by filling the tube with mercury through a series of pressurization steps.

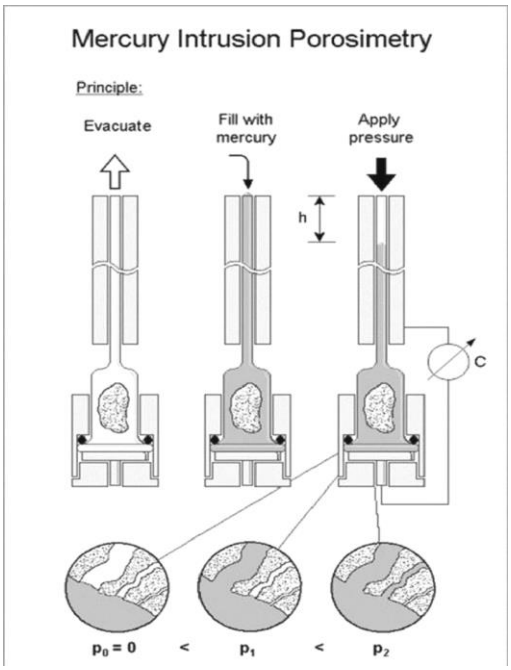

Figure 2.2: Schematic diagram of the MIP test for pore volume measurement [Penumadu and Dean, 2000].

There are several sources of error in the MIP test, which originate from sample size and shape, operating conditions, mercury and penetrometer properties. This method also has some disadvantages which limit its usage. A list of these errors and disadvantages is provided below [Mcphee, et al., 2015]:

- If the rock sample has low mechanical strength, it may be flattened or collapsed when exposed to high pressure. Considering the compressibility of mercury and the glass container, greater pressure values may also distort the rock sample and create induced pores which were not already present in the pristine porous sample before the MIP test.
- A small sample size is prone to measurement errors in both pore volume and bulk volume measurements using mercury intrusion.
- The penetrometer movement from the low to high pressure chamber may introduce error in the form of spikes in the data since wrong volume of mercury maybe reported.
- Errors can also be originated from mercury density instability, contaminated mercury, or improper sample drying procedure.
- The contact angle and interfacial tension (IFT) might not be representative of that of the reservoir oil-brine interface, therefore, there is a need for suitable conversion from air (or mercury vapor)-mercury to oil/gas-brine in estimating initial fluid in place.
- The MIP test is destructive because the mercury intruded into the pore structure cannot completely be removed, and the sample cannot be used for another test. The capillary pressure measurement using mercury intrusion requires a conversion factor, focusing on fluid pair difference from MICP to real reservoir condition.
- This method does not measure closed porosity (i.e., porosity of isolated pores).

There are some advantages associated with the use of mercury for porosimetry which are given below [Haugen and Bertoldi, 2017]:

- MIP is an inexpensive method,that provides pore volume information over a short duration of testing.
- The results obtained from MIP method are independent of the porous sample orientation.
- This method can be applied for low permeability samples as well, with a maximum testing pressure of approximately 60,000 psig.
- This method can be used on core plugs, off–cut samples or cuttings.
- The pore size and pore volume values measured using the MIP method are repeatable to about 1% standard deviation. In some cases, the results from this method are in satisfactory agreement with those of other methods such as image analysis and water absorption. A broad pore size distribution of 0.003 to 360 micrometers can be determined using the MIP method
- Using the MIP method, both the through-pores and closed pores can be detected and included in the total porosity value measurement. In addition, both the inter-particle pores (i.e., the pores between the individual particles) and the intra-particle pores (i.e., the pores within the particle itself) can be characterized.

It is possible to develop correction correlations based on which the porosity (and calculated permeability) values from the MIP method could be converted to values based on more accurate methods such as gas porosimetry and permeametry. This is the main objective of this research work. Some other corrections are also needed (and are part of the routine MIP data analysis) to account for the effect of mercury pressure-volume, closure, and clay-bound corrections.

2.1.1.2 Image Analysis

Image analysis is predominantly used for pore structure analysis and characterization. The 2D and 3D image analysis techniques use backscattered images to estimate porosity. Through the image analysis technique, porosity of a sample is estimated by executing image thresholding for the captured backscattered electron microscope images. Generally, porosity changes from micro to macro level, which causes uncertainty in estimation of porosity using this method [Pal A. et al., 2018].

2.1.1.3 Helium Pycnometry

Gas pycnometry is a non-destructive technique which applies the principle of gas expansion to accurately measure the pore volume, making it an accurate yet simple method for measuring porosity and grain density. In this method, a sample of known weight is sealed in the sample compartment, which is maintained at a constant temperature. Helium is then added from a source compartment (with known pressure and at a constant temperature) into the sample compartment. The sample compartment pressure is closely monitored, and the stabilized pressure is used with Boyle's gas law to calculate the sample pore volume. The small size of the helium molecules with an atomic radius of 0.208 nm enables them to penetrate into the sample pores. The test is concluded by releasing the pressure from the sample compartment and removing the sample [Merlin Powder Characterization, n.d.].

2.1.1.4 Saturation Technique

In this method, the porous sample is dried to a constant weight, and the weight is recorded. The sample is then evacuated, and then pressure saturated with either water or light hydrocarbon. The difference in weight between the saturated and dry sample is the weight of the fluid occupying the pore space. The pore space is the ratio of the mass difference to the density of the fluid used. This

method is slow and slightly difficult to properly execute. It is also required that the fluid used do not react with the porous medium surfaces. Incomplete saturation could occur which produces erroneous low porosity data. It is non-destructive as the sample can be reused for other tests. This method is usually used as a quality control check in special core analysis test (Petroshine, n.d)

To summarize, the porosity measurement methods introduced in this section are compared to each other in the below table:

Table 2.1: Comparison of porosity measurement methods [Fernanda et al., 2000].

Method	Advantages	Disadvantages
Mercury porosimetry	Can measure open porosity with excellent precision Can be used on core plugs, off–cut samples or cuttings	Cannot determine closed porosity The test is destructive
Image Analysis	Can determine pore size distribution and pore morphology	Cannot distinguish between closed and open pores Uncertainty in estimation of porosity
Helium pycnometry	Can determine both open and closed porosity Can be used to determine grain density	The results could contain some errors if dead volume is not taken care of. Incomplete cleaning will yield lower porosity values
Saturation Technique	Inexpensive Porosity results could be used as a quality control method for special core analysis	It is a slow process Incomplete saturation results in unreliable measurements

2.2 Permeability

Permeability is the measure of a rock's ability to transmit fluids. It indicates the interconnectivity of the pore space. Porosity and permeability describe the rock's ability to hold and transmit fluid, respectively. An underground reservoir can be porous, but if the pores are not interconnected, the permeability is low, and the fluid will be trapped. In permeability measurement, the ability of the porous medium to transmit a single-phase fluid is called absolute permeability; however, the ability of the porous medium to transmit fluid i in the presence of other fluids is called effective permeability to fluid i. Permeability is expressed in millidarcy (mD, filed units), and is measured using different methods in the lab such as gas permeametry, liquid permeametry and MIP. Note that the permeability values obtained from the MIP method are not direct measurements, but rather are calculated values based on a correlation that uses the capillary pressure and pore throat size distribution obtained from the MIP test.

2.2.1 Permeability Measurement Methods

Permeability of a rock sample can be measured using the following methods in the lab:

2.2.1.1 Mercury Porosimetry

Using mercury porosimetry, the porosity, pore size distribution, and injection pressure versus saturation of mercury in the rock sample are directly obtained in the lab. The pore size distribution and mercury pressure vs. saturation information can then be used to calculate permeability of the rock sample. For instance, Katz and Thompson model is used in 9500 Autopore IV Porosimeter for permeability calculation. For further information on how to operate the mercury porosimeter, please refer to section 2.1.1.1.

2.2.1.2 Gas Permeametry

In this method, a gas phase flows through the rock sample under steady state condition, and the rock permeability is calculated using Darcy's law by having the pressure differential across the flow length, gas flow rate, and some gas physical properties. Compared to the use of liquids, a gas phase has a finite velocity at the sand grain surface; therefore, the permeability value obtained using a gas phase will be often greater than the values when a liquid phase is being used. To correct the gas permeametry data, Klinkenberg [1941] proposed a correction factor by introducing the following gas permeametry and data analysis protocol: The permeability measurement is carried out using a gas phase at various gas flow rates while recording equilibrated pressure differential across the rock sample. Plotting the gas permeability versus $1/P_m$ (P_m is the mean pressure) results in a linear trend. By extrapolation the linear plot to zero (0) on the x axis, the so-called "Klinkenberg-corrected permeability" is obtained as the y-intercept, which is equivalent to the liquid permeability at infinite mean pressure value. This procedure is demonstrated in Figure 3 in which three different gases were used to measure a core sample permeability. When the Klinkenberg correction was applied at infinite mean pressure for gas permeametry data, all three tests exhibited the same permeability value as that of the liquid permeametry test.

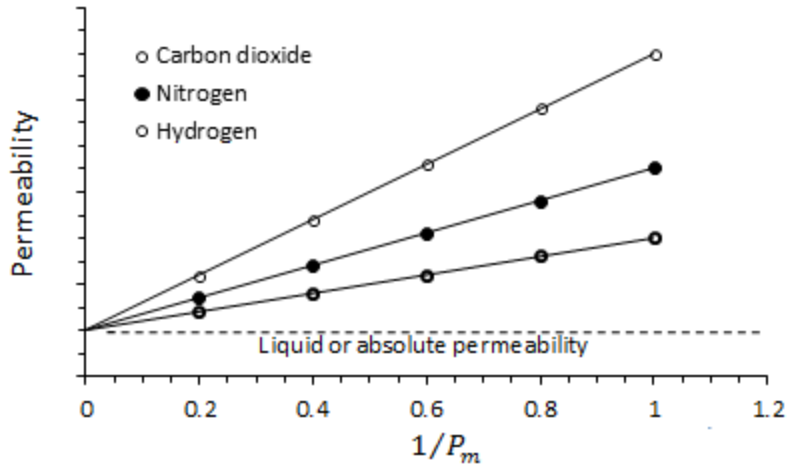

Figure 2.3:Effect of gas type and mean pressure on gas permeametry of a core sample – the liquid permeability is presented as a reference [Perm TIPM Laboratory, 2018].

The above method is a steady-state gas permeametry method. There is another class of permeametry methods, the so-called transient methods that differ in implementation and data analysis from the steady state method. These methods include pulse decay permeametry and pore pressure oscillation method, to name a few.

2.2.1.3 Pulse Decay Permeametry

Pulse decay permeametry is often used to analyse core plugs extracted from unconventional plays. It is a faster and more accurate method than steady state method for low permeability cores (i.e., up to 1nD). The test could be done at a confining pressure of up to 10,000 psig, and can be designed for either gas or liquid flow. Shale/mud-rock samples are often tested at as-received water saturation, resulting in effective k_g or k_o. This method produces gas permeability at high pore pressure, thus greatly reduces the Klinkenberg slippage. It also needs a low differential pressure across the sample, thus no inertial effects [Brace et al., 1968; Jouniaux et al., 1994]

2.2.1.4 Pore Pressure Oscillation Method

Similar to the pulse decay method, the pore pressure oscillation method is applied for measuring permeability of tight porous media samples for which it takes extremely long time to reach stable flow rate – pressure conditions to implement steady state permeametry. This method is based on introduction of a regularly-oscillating pressure condition at one end of the core sample while the transmitted fluctuation is analysed at the opposite edge of the core sample. Contrary to the pulse decay method, the pore pressure oscillation method can also be used for high permeable samples. This method was applied to low permeability claystone plugs with permeabilities of up to 2 nD [Metwally and Sondergeld 2011: Ismael and Jacobo, 2013].

In summary, the permeability measurement methods are compared in Table 2 with advantages and downsides associated with each method.

Table 2: Comparison of permeametry methods [Badrouchi et al., 2019].

Method	Advantage	Disadvantage
MIP	Cheap and fast	Several errors could affect the measurement. It also does not directly measure the permeability.
Air Permeametry	Gas, unlike water, does not react with rock constituents (i.e., clays), so it is a non-destructive permeametry method.	Need correction for Klinkenberg effect.
Liquid permeametry	Results in direct and more accurate permeability data	Clay swelling when fresh or low-salinity aqueous phase is used. Therefore, it could be destructive depending on the mineralogy and aqueous phase composition. Scaling in the injection line could occur when fresh or low-salinity water is used.

2.3. Capillary Pressure

Capillary pressure (Pc) is the pressure difference between two immiscible fluids in contact with each other, which occurs because of the force interaction between the fluids and their surrounding solid surfaces [Dimri and Nimisha, 2012]. According to Anderson [1986], wettability is defined

as the "tendency of one fluid to spread on or adhere to a solid surface in the presence of other immiscible fluids". In a rock/oil/brine system, it is a measure of the preference that the rock has for either the oil or water. This concept is demonstrated in Figure 2.4

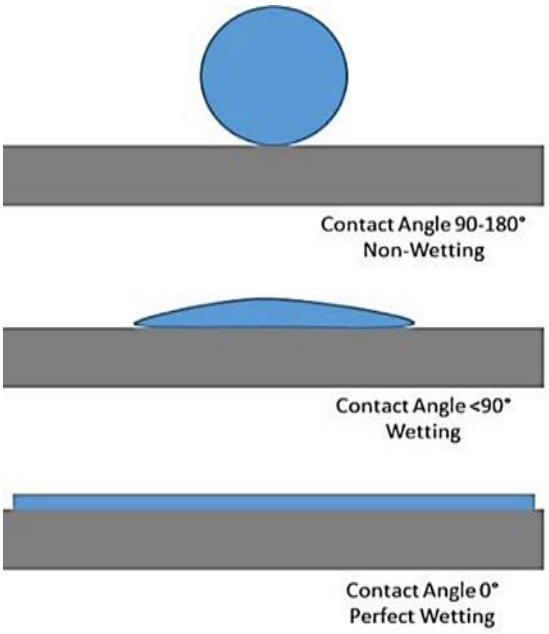

Figure 2.4: Wettability determination using contact angle measurement modified from [Wong, 2017].

The top illustration shows the ball-shaped liquid droplet sitting on top of the solid surface, which does not spread over the surface, meaning the liquid in this scenario is a non-wetting phase for this particular solid surface forming a contact angle of 90-180°. However, in the middle illustration where the liquid phase partially wets the solid surface, some of the liquid can spread across the wall with a contact angle of <90° and it is a wetting fluid. The bottom illustration shows perfect wetting of the solid surface with the liquid film, with a contact angle of 0°.

Capillary pressure is represented mathematically using the Young-Laplace equation. For spherical interfaces, formed in sufficiently narrow capillary tubes with circular cross section, the

capillary pressure (C_p) that exists between the interface of two immiscible fluids is caused by surface tension. The capillary pressure is expressed as [Mahmound et al., 2007]:

$$C_p = \frac{2\gamma cos\theta}{a} \, . A \qquad \text{Eq 2.2}$$

where C_p is capillary pressure (psig), γ is interfacial tension (dynes/cm), $\theta \; is$ contact angle (degrees), a is pore radius (microns), and A is a constant = 145×10^{-3} [Mahmound et al., 2007].

2.3.1 Capillary Pressure Measurement Methods

There are four common methods to measure capillary pressure: centrifuge method, porous plate method, mercury injection method, and vapor desorption method. These methods are described in the sections below.

2.3.1.1 Centrifuge Method

Each core plug sample should be thoroughly characterized in terms of porosity, permeability, and initial water saturation. Under centrifugal force, the core plugs undergo drainage displacement process which is controlled by capillary forces. The core plugs saturated with water are loaded in special core holders, along with oil, i.e., the displacing fluid. The core holders, water saturated core plugs, as well as the displacing fluid (i.e., oil) are spun at different rotational speeds, which causes the denser fluid (i.e., water in this drainage displacement case) to be forced away from the center of rotation while the lighter fluid (i.e., oil) moves toward the center of rotation. The fluid phase expelled from the core plug sample is then collected in a graduated tube for accurate volume measurement (i.e., ≤ 0.01cc) using a high-accuracy camera or stroboscope attached to the system [McPhee et al., 2015]. The rotational speed is increased stepwise, and each speed is kept constant until no more displaced phase is expelled from the core plug, ie saturation equilibrium is achieved

at that stage. The saturation equilibrium at each particular rotational speed occurs when the volume of the expelled liquid collected in the graduated tube remains unchanged. With the values of pore volume and volume of expelled liquid phase (i.e., water), water and oil saturations can be calculated. Researchers have developed various assumptions and mathematical models to calculate average expelled water volume. The reverse process can also be done to generate the imbibition capillary pressure curve. Therefore, the full cycle of capillary pressure curves can be obtained using the centrifuge technique. It is essential to keep the fluids produced during the drainage process in contact with the sample while decreasing the speed of rotation, to allow that fluid to imbibe spontaneously step-by-step (i.e., positive imbibition). During the experiment, an oil-water interface is constantly detected and maintained at the outlet face of the sample using an external non-rotating pump connected to the core holder through a rotating fitting. The average saturation is then deduced from the volume pumped in and out of the core holder [Fleury et al., 2001, Champion and Davy, 1937; Bruce et al., 1947].

2.3.1.2 Porous Plate Method

In this experiment, a clean sample of known porosity is saturated with a wetting fluid phase and then placed in the porous plate that is permeable to the wetting phase (i.e., a membrane with average pore radius of <1 micron). Using the porous plate method, there is continuity between the wetting phase content of the core plug and that below the membrane. A non-wetting phase is then forced into the sample through stepwise pressure application to facilitate a drainage process [Mcphee et al., 2015]. At one point, the applied incremental pressure on the non-wetting phase becomes great enough at which it invades through the rock pore space but not that of the membrane. This results in the drainage of the wetting phase out of the rock sample and through the membrane for saturation measurement. The changes in saturation are determined after

equilibrium is reached during each pressure step. At the end of the drainage process, the sample is removed from the cell, and the residual water saturation is determined by comparing with the initial sample's dried weight. The process of displacement by fluid injection is often reversed before the capillary pressure reaches the threshold pressure of the plate. By decreasing the pressure in the chamber in small steps, the capillary pressure curve for imbibition can be determined. During the capillary pressure measurement test, the continuity between the specimen and membrane should be maintained, which is governed by the sample's shape [McPhee et al. 2015]. The capillary contact may be lost for samples with rough surfaces or irregular shapes, causing water to be trapped between the specimen and membrane resulting in inaccurate saturation measurement. This can be determined by comparing the results obtained from porous plate method with those from other capillary pressure measurement methods.

2.3.1.3 Mercury Intrusion Capillary Pressure (MICP) Method

In MICP method, the mercury volume invading through a pore space is measured at incremental mercury injection pressure. Mercury does not wet the rock, so the Hg pressure is directly applied in measuring capillary pressure. The effective pore throat(s) diameter is calculated from the mercury injection pressure obtained from the MICP test using Young-Laplace equation. Knowing the mercury surface tension and wettability and assuming cylindrical geometry for the average pore-throats, the pore throat diameter can be calculated using the following equation:

$$D = \frac{4Tcosq}{Pc} \qquad \text{Eq 2.3}$$

where q is contact angle (^{o}), T is surface tension (N/m), P_c is capillary pressure (Pa), and D is cylindrical pore throat diameter (m) [Jang et al., 2016].

A schematic diagram of intruded and extruded mercury volume as a function of applied pressure is illustrated in Figure 3. An important observation from this figure is the difference

between the intruded and extruded mercury volume as a function of the applied pressure, as well as its maximum value at zero pressure (i.e., start of the saturation process and endpoint of the desaturation process) that exhibits mercury entrapment in the test sample. This signifies the destructive nature of the MICP test. When mercury porosimetry was used for weak compressibility sandstone samples with permeability values greater than 1×10^{-15} μm^2, it was reported that the saturation data error caused by the compression effect can be neglected [Shafer & Neasham, 2000]. The capillary pressure results obtained from the MICP test are primarily useful in comparative studies of similar materials [Adam et al., 2015].

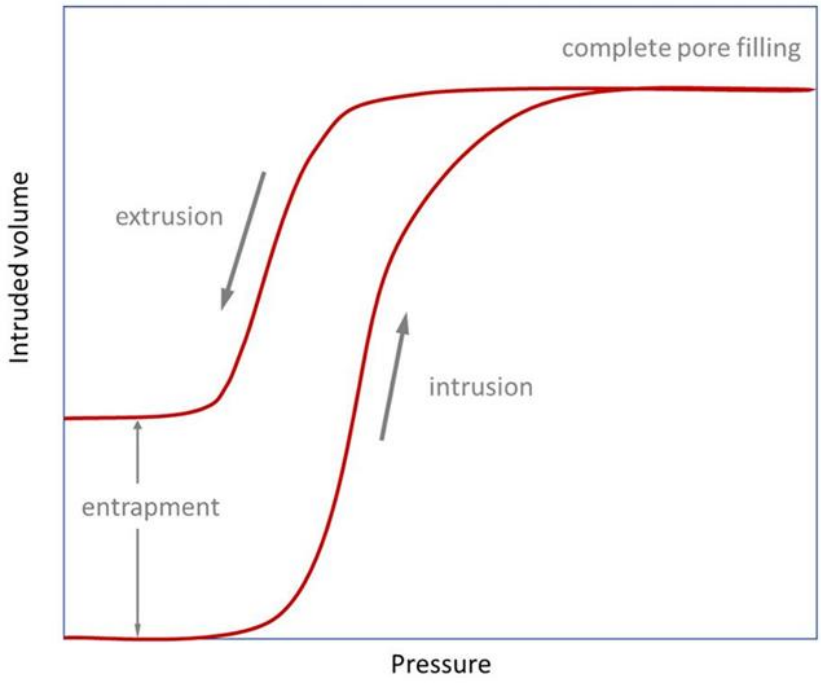

Figure 2.5: Capillary pressure curves obtained from the MICP test showing mercury entrapment in the test sample [Anton Parr, 2010].

2.3.1.4 Vapor Desorption Method

Dynamic vapor sorption (DVS) method uses gravimetric analysis to measure the rate and quantity of solvent absorption in a sample. A relationship exists between the curvature of a gas-liquid

interface and the vapor pressure of the liquid phase. Since the interface curvature is directly related to the capillary pressure across the interface, it is possible to determine the capillary pressure with measuring the vapor pressure reduction associated with a curved interface [Melrose, 1988]. This relationship has been incorporated in the form of the renowned Kelvin equation.

In Table 3, the methods introduced in this section for capillary pressure measurement are compared, with a list of advantages and downsides mentioned for each method.

Table 2.3: Comparison of different methods for capillary pressure measurement [modified from McPhee et al., 2015].

	Porous Plate	Mercury Porosimetry	Centrifuge	Vapor Desorption
Testing time	Long (30-50 weeks)	Quick (some hours)	Quick (about 2 weeks)	Not quick (up to 1 month)
Testing fluid	Stock tank oil (STO), brine, or synthetic fluids	Mercury	STO, brine	liquid, gas
Porous medium	Permeable rock samples, clay-rich specimen	Suitable for most rock types and cuttings; some clay effects; well suited for low permeability samples	Suitable for most rock types	Good for most rock types
Porous medium preservation	Non destructive	Destructive	Non destructive	Non destructive
Cost	Expensive, but less than centrifuge method	Inexpensive	Expensive	Expensive
Operating condition	HPHT reservoir conditions	Laboratory conditions	HPHT reservoir condition (up to 647 psig and 90°C)	Laboratory conditions
Representativeness	Thin gas and oil column	Thick gas and oil columns	Requires high spin speed to represent a thick hydrocarbon column	Thin gas and oil column
Disadvantages	Lengthy, expensive, capillary equilibrium issues.	Destructive, Hg is not a strong wetting phase, non-representativeness of the testing fluids	Expensive, rock sample under excessive stress which could cause induced fractures, inaccurate and time-consuming	Test requires constant-humidity environment
Additional Advantages	Can measure rock resistivity at capillary equilibrium	Provides information on pore throat size distribution, rock typing, imbibition and drainage curves	Obtaining the desaturation curve is more rapid than with porous plate method	Particularly suitable for low-saturation, high-pressure region of the capillary-pressure curve.

Chapter 3: Literature Review

One of the most important reservoir rock properties is permeability. It can directly be measured using methods discussed in Chapter Two. For decades, researchers have also worked on methods to predict reservoir rock permeability based on other rock properties. Various models have been proposed based on grain size, pore size, and surface area. Permeability is also estimated from petrophysical well logs. The porosity-permeability cross plot is also frequently used, although this approach for rock typing has some errors [MacDonald, 2020]. Among the methods involving lab measurements and empirical modelling for permeability determination, mercury intrusion porosimetry (MIP) has been tested extensively in the literature. In the following sections, a summary of these applications is provided.

In 1921, Washburn proposed the use of mercury injection to determine effective pore throat size distribution based on the following equation which was initially applied to study charcoal, but was later adopted for reservoir rock characterization in the petroleum industry [Washburn, 1921].

$$r = \frac{2\sigma cos\theta}{P} \qquad \text{Eq 3.1}$$

where σ stands for mercury surface tension, θ is contact angle, and P is the average capillary pressure value for the effective pore throat diameter.

The model developed by Washburn (Eq 4) has been applied by different researchers for porous media characterization, including Leverett [1941], Purcell [1941], Thomeer [1960] and Swanson [1981], to name a few. For instance, the Washburn correlation was used by Purcell [1941] for capillary pressure curves obtained from the MICP test. The MICP protocol was also modified in this study, in that an upright sample chamber was used, and the pressure was corrected for hydrostatic pressure caused by the mercury column. The concept of flow through capillary tubes were utilized to simulate fluid flow in porous media. For that, Poiseuille's equation was used

assuming there are N parallel capillary tubes making up the network, consisting of the same length but of different diameters. The results were then compared against calculations done by Darcy equation. Finally, a lithology factor (i.e., *F*) was introduced to correct for the representation of actual porous medium as a bundle of capillary tubes. A correlation was then suggested to estimate permeability based on the mercury porosimetry data:

$$k = 0.66F\phi \int_0^1 \frac{dS}{P_c^2} \qquad \text{Eq 3.2}$$

where S is the mercury saturation in the rock sample, ϕ stands for porosity, and P_c is capillary pressure.

Thomeer [1960] investigated the shape of capillary pressure curves obtained from the MIP test. It was concluded that pore geometry is responsible for the differences in shape and relative distance of the capillary pressure curves with respect to the axes. The distance of the curve with respect to the volume axis was considered as a measure of "interconnected pore volume" whereas the relative distance of the curve with respect to the P_c axis was interpreted as the pore cross-sectional area that was first intruded by mercury. The shape of capillary pressure curve was also used to determine the level of pore interconnection and sorting. In addition, a correlation was developed to describe MP data as a function of threshold capillary pressure, mercury saturation at infinite capillary pressure, and pore geometric factor as follows:

$$B_v = B_\infty exp(-G/log(P_c/P_d)) \qquad \text{Eq 3.3}$$

where P_c is the capillary pressure in psig, B_v is the volume fraction of mercury injected into a porous rock sample in fraction, P_d is the extrapolated displacement pressure in psig, B_∞ is the percent bulk volume occupied by mercury at infinite capillary pressure in fraction, and G is the pore geometrical factor in dimensionless units.

Another classic work in relating permeability to capillary pressure data, derived from the MICP test, was reported by Swanson [1981], in which the MICP data was plotted as a hyperbolic curve (i.e., log-log plot of the percent bulk volume occupied by mercury, S_b, versus capillary pressure). It was obtained that the apex of this curve often coincides with the inflection point of the initial-residual saturation curve. This inflection point was described by Swanson as a moment at which the non-wetting phase distribution undergoes transition from "broadening spatial distribution and trapping" to "fine structure trapping and/or intrusion into pore corners", which represents the pore space proportion that contributes to the fluid flow. Therefore, the capillary pressure at the apex point can be used to determine the pore size connecting the effective pore space, hence permeability can be determined [Apisaksirikul and Blasingame, 2016]. Swanson also developed a correlation between the effective pore throat diameter and air and brine permeabilities. The effect of sample size on the P_c curve apex value was also studied by using core plugs as well as drill cuttings in the MICP measurements, and the impact was found insignificant. The permeability-capillary pressure data relationship was proposed in the following form:

$$k = a(S_b/P_c)^c_{max} \qquad \text{Eq 3.4}$$

where k is permeability, a and c constants depend on the rock type (i.e., carbonate or sandstone) and fluid type (i.e., air or brine), respectively, and S_b is the percent bulk volume occupied by mercury.

The Swanson model was then widely applied in the literature, and various modifications were proposed based on different rock and fluid systems. For instance, Guo, et al. (2004) improved the Swanson's model by introducing a parameter called "capillary parachor" which describes the rock pore structure, hence strongly depends on rock permeability. When plotting the percentage of bulk volume occupied by mercury (S_b) versus squared capillary pressure, the capillary parachor

defined as $(S_b/P_c^2)_{max}$ is the maximum height of the cross plot. The permeability can then be calculated using the following correlation:

$$k = C * (S_b/P_c^2)_{max}^D \quad \text{Eq 3.5}$$

where C and D are constants.

Although the original Swanson model as well as its Guo et al. modification have been widely used in estimating permeability from the MIP data, Liu et al. (2016) presented an argument against their reliability. According to Liu et al. (2016), both the Swanson Parameter and Parachor parameter have poor relationship with rock permeability. In an effort to improve on these two models, Liu et al. (2016) introduced "porosity" into capillary parachor model as outlined below in a general form:

$$k = a_0\phi^{a1} * a(S_b/P_c^2)_{max}^D \quad \text{Eq 3.6}$$

where ϕ is porosity in %, and a_0, a_1 and D are model parameters.

Liu et al. (2016) then calibrated the model (Eq 9) using information from 30 core samples, and obtained the parameters as shown in the below equation:

$$k = 10^{-5.129}\phi^{3.141} * (S_b/P_c^2)_{max}^{0.876} \quad \text{Eq 3.7}$$

Saki et al. (2020) used the MIP data of 187 sandstone, limestone, and dolomite core samples to develop a new generalized equation to estimate uncorrected gas permeability. In this research work, the authors used the smallest pore/throat radius invaded by mercury at a mercury saturation of 35% pore volume, and proposed the following equation for permeability estimation based on the MIP data:

$$logk=0.0583+1.4660log\ r_{35}+0.6993log\ \phi \quad \text{Eq 3.8}$$

where k is gas permeability (mD), ϕ denotes porosity (%), and r_{35} is the smallest pore/throat radius that is filled by mercury at 35% mercury saturation (μm).

Saki et al. (2020) then compared their permeability predictions with those obtained using other correlations (i.e., Gao and Hu (2004), Rezaee et al. (2012), Pittman (1992), and Katz and Thompson (1986)), and concluded that in general, the permeability predictions using Eq 11 were more accurate compared to other correlations when compared against the experimental data.

Some advantages and shortcomings of permeability correlations based on the MIP data are presented in Table 4. From the literature review provided in this section, it is clear that even though there are various correlations developed in the literature to estimate permeability based on mercury intrusion porosimetry data, there are still significant differences between the estimated versus measured permeability values. Therefore, the permeability data obtained from mercury porosimetry (i.e., correlation-based) should be corrected with reference to a more accurate direct permeability measurement, such as gas permeametry method. This is the topic of this research work

Table 3.1: Comparison of different correlations for permeability estimation using mercury porosimetry data

Purcell (1941)	Swanson (1981)	Guo, et al (2004)	Liu et al. (2016)	Saki et al. (2020)
Estimates air permeability based on mercury intrusion data. Can be applied to small and irregular shaped rock samples. Difficult to get all the model parameters.	Uses the relationship between capillary pressure and Hg saturation for permeability estimation. Permeability can easily be computed from the MICP data. This method is more accurate for some rock types such as those with high permeability. It has poor predicting performance according to Liu et al.	Improved the Swanson's model by introducing the capillary parachor. It has poor predicting performance according to Liu et al.	Improved on Swanson and Guo et al. model by introducing porosity into capillary parachor parameter. More parameters are needed.	uses the smallest pore/throat radius invaded by mercury at a mercury saturation of 35% pore volume. Saki et al. claim that this model has higher accuracy compared to other models.

Chapter 4: Methodology

4.1 Work Plan

In this work, nineteen (19) sandstone samples from Hibernia B16-17 well, drilled offshore NL (Canada) were analysed for permeability and porosity using MIP method with 9500 Autopore IV Porosimeter equipment as well as air permeametry method. The core plug samples were drilled from a homogeneous full core, collected from 3955.50.40 – 4099.95 m depth interval. The MIP test was used for porosity measurement and permeability estimation. A single plug coreflooding setup was also used to measure gas permeability, followed by Klinkenberg correction. Some porosity measurements, using helium pycnometry, were done by Core Laboratories Inc. [1999] on several core plugs from the same depth range as that of the samples used in this research work. For the comparison purposes, the pycnometry results were borrowed from a publicly available database. The depth information associated with these porosity values correspond with the depths associated with the core plug samples tested in this research work. It should be noted that the sample labels given in the Core Laboratories report [1999] differ from the labels assigned to the samples tested in this study, but the sample depth intervals are the same.

4.2 Core Sample Information

A summary of core plug samples used in this study is provided in Table 4.1. Two samples were selected for quality assurance purposes for which the air permeametry and mercury porosimetry tests were repeated.

4.3 Porosity and Capillary Pressure Measurements Using MICP Test

Using 9500 Autopore IV Porosimeter, porosity and mercury intrusion results (i.e., mercury intrusion pressure and intruded volume) were measured. A snapshot of the equipment is shown in Figure 4.1.

Table 4.1: Summary of core plug samples and testing details

Sample ID	Depth (m)	Permeability		Porosity	QA Sample
		MIP (Estimated)	Air Permeametry (Measured)	MP	
SP 1	3959.40 - 3959.79	✓	✓	✓	
SP 3	3961.85 - 3962.32	✓	✓	✓	✓
SP 4	3967.28 -3967.98	✓	✓	✓	
SP 5	3970.33 - 3970.67	✓	✓	✓	
SP 6	3970.96 - 3971.20	✓	✓	✓	
SP 7	3973.29 - 3973.58	✓	✓	✓	
SP 8	3978.57 - 3979.29	✓	✓	✓	
SP 10	4009.40 - 4009.60	✓	✓	✓	
SP 13	4017.54 - 4017.80	✓	✓	✓	
SP 14	4020.98 - 4021.28	✓	✓	✓	
SP 17	4027.94 - 4028.17	✓	✓	✓	✓
SP 18	4035.83 - 4036.08	✓	✓	✓	
SP 19	4037.15 - 4037.49	✓	✓	✓	
SP 20	4040.31 - 4040.52	✓	✓	✓	
SP 22	4043.20 - 4043.39	✓	✓	✓	
SP 23	4045.73 - 4046.05	✓	✓	✓	
SP 30	4082.12 - 4082.34	✓	✓	✓	
SP 31	4083.86 - 4084.10	✓	✓	✓	
SP 32	4088.01 - 4088.37	✓	✓	✓	

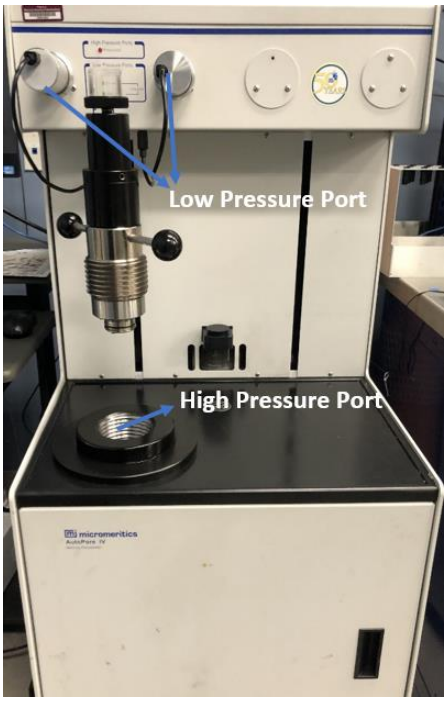

Figure 4.1: A snapshot of 9500 Autopore IV Porosimeter used in this study.

Details of measurement procedure were discussed in Section 2.2.11. The equipment was first calibrated using standard sample of silica Alumina labelled 004/16822/00 REF MAT. When the measurement reliability was confirmed by testing the standard sample, mercury intrusion tests were conducted on small segments cut out from each core plug sample. In order to test the repeatability of measurements, the MIP test was done on three small segments cut out from each of SP3 and SP17 samples. The repeatability analysis was performed by calculating some statistical measures (average, standard deviation, confidence interval, and coefficient of variation). Another check on validity of the MIP measurements is the percentage volume of the stem used for each test. The reported MIP results in this study all have used a stem volume of 25 - 90%, which is the requirement for this test/equipment standard operating procedure in order to consider the results "valid".

4.4 Permeability Measurement Using Gas Permeametry Tests

In this method, which is in accordance to ASTM 4525, the core sample is first prepared for testing by cutting to a cylindrical shape and trimming the edges, followed by cleaning by solvent(s) in Soxhlet unit and then drying in a convection oven at 60°C to a constant weight. A gas phase was flowed through the rock sample under steady-state conditions, and the rock permeability was calculated using Darcy law by having the pressure differential across the flow length, gas flow rate, and some gas physical properties. A schematic diagram of the setup used for gas permeametry is shown in Figure 7(a), and a photo of the actual setup is shown in Figure 7(b). The dimensions of cleaned/dried core plugs were accurately measured with a caliper, and the bulk volume was calculated using geometrical method. Each single core sample was loaded into a core holder. An overburden pressure of 400 psig was applied with the manual hydraulic pump. The outlet valve, acting as a BPR in all the gas permeametry tests, was open, and the nitrogen gas flowed through the system to displace the air out and maintain a steady state gas flow for permeability measurement. Before applying a back pressure, the inlet pressure, P_1 (through the inlet valve), and differential pressure (DP) were maintained constant with a very small variation of ± 0.003 psig per min. This was done by regulating the pressure relief valve. When both P_1 and DP were stabilized, the relief valve was closed, and the pressures and flow rate were allowed to re-stabilize. The pressure value was considered "equilibrated" when its value remained within ± 0.003 psig change over a 1-minute interval. The flow rate was considered "equilibrated" when its variation remained within 1 ml/min change over a 1-minute interval. The back pressure was applied by closing the outlet valve, thereby slightly increasing the P_1. The stabilized flow rate, injection pressure, and differential pressure were recorded for each permeametry test. This was repeated for 4 pressure steps to execute the 5-points Klinkenberg corrected permeability determination. The calculated

gas permeabilities (K_g) at various flow rate and pressure conditions were plotted against the inverse of mean pressure ($1/P_m$). A linear correlation was fitted into the data points, and then extrapolated to zero inverse mean pressure value (i.e., y-axis intercept at infinite mean pressure) to obtain the Klinkenberg-corrected permeability, which is known as the equivalent liquid permeability of the tested sample. To check the reliability of experimental setup and gas permeametry protocol, a standard sample, S359, with known permeability value, was tested. A sample gas permeametry calculation for SP13 specimen, along with associated graphs and data for all the tested samples are presented in Appendix A.

4.5 Porosity Results Obtained from Literature

Samples from Hibernia B16-17 well, collected from the same depths as those of the samples analyzed in this study, were analysed by Core Laboratories for porosity using helium pycnometry [Core Laboratories, 1999]. The results were retrieved from CNLOPB public databases and used in this study for comparison purposes against porosity measurements using the MIP test.

4.6 Estimation of Permeability by Swanson Model

The following form of the Swanson model was used in this study in order to estimate permeability from the MIP data [Babak et al., 2014]:

$$k = a(S_b/P_c)^c_{max} \qquad \text{Eq 4.1}$$

where k is the permeability (mD), S_b is mercury saturation (mg/g), and P_c is mercury injection pressure (MPa).

Considering the wetting phase and sample lithology in this study (i.e., air and sandstone, respectively), the constants a and c in Eq 4.1 are 399 and 1.691, respectively. The Swanson parameter $(S_b/P_c)_{max}$ is the apex of the S_b/P_c (ratio of mercury saturation to pressure) against S_b % (percentage volume of pore space occupied by mercury) (Xiao et al., 2014). A sample permeability

calculation using the modified Swanson model for SP8 sample based on the MIP data is presented in Appendix B, along with the associated plots for all other samples tested in this study.

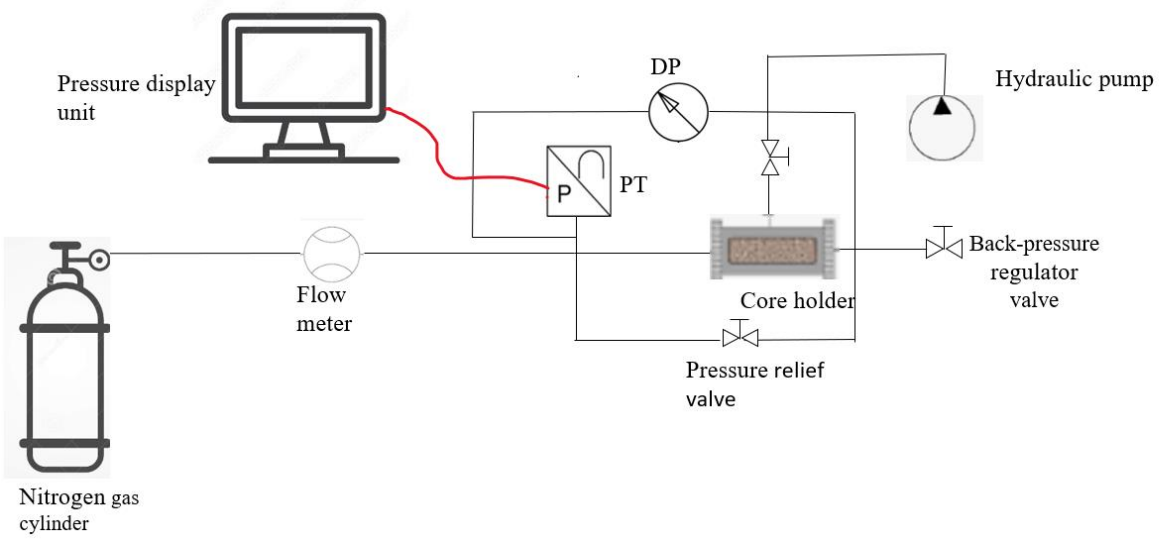

(a)

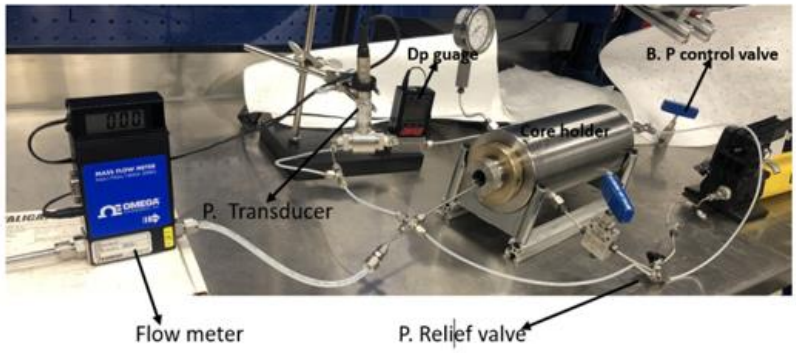

(b)

Figure 4.2: Schematic diagram of gas permeametry setup

4.7 Comparative Analysis of Results

The permeability values calculated based on the MIP data were compared against the Klinkenberg-corrected gas permeability data as well as those estimated using Swanson model. The porosity values measured using mercury porosimetry were compared against the porosity data from helium pycnometry obtained from the literature. Among all the permeametry measurement / calculation

methods described in this study, liquid permeametry and gas permeametry seem to be the most reliable methods [Waszkiewicz, S., 2019]. The percentage differences were computed. The Bland-Altman (B&A) plots were prepared for these comparative analyses, which display the relationship between two paired variables using the same scale and provide errors and bias. These plots were prepared by computing the difference between values from different methods and plotting it against their average value. It is believed that a plot of the difference between the methods (A-B) against (A+B)/2 provides easier assessment of the magnitude of disagreement (both error and bias), spotting outliers, and exploring any possible trends. According to the principle behind the B&A plots, 95% of the data points should lie within ± 2 *standard deviation* of the mean difference [Giavarine, 2015].

Chapter 5: Results and Discussion

5.1 Determination of Core Plug Permeabilities

The core plug permeabilities were measured or calculated using various methods in this study. A) A gas permeameter setup was used to directly measure permeability of 19 core plug samples (Table 4.1) using nitrogen gas at lab temperature. For this purpose, a reference core plug sample with known permeability was first tested to assess reliability of the setup and validate the permeability measurements. Once validated, the gas permeability of all 19 core plugs were measured at various mean pressure values, followed by corrections for the gas slippage effect to obtain Klinkenberg-corrected permeability. B) The core plug permeabilities were calculated using MIP data. For this purpose, a standard sample was first used to assess the reliability of the setup and validate the measurements. Once validated, small quantities of rock materials extracted from each core plug were used for the mercury intrusion tests. The pore size distribution and applied mercury pressure used in these tests were used by the instrument for permeability calculation using Katz and Thompson model. C) A widely-accepted correlation, known as modified Swanson model was used to estimate core plug permeabilities based on mercury capillary pressure data measured using the MIP tests. The permeability data obtained using these three methods were then compared, and some statistical analyses were conducted to highlight the differences.

5.1.1 Gas permeametry using nitrogen at lab temperature

In order to assess the reliability of gas permeability measurements and quality check the data, a standard core plug sample (S359) with known permeability was tested with the assembled gas permeametry setup at four mean pressure values. The Klinkenberg correction for gas permeametry done on reference sample S359 is illustrated in Figure 4.3. At each mean pressure, gas permeability was calculated using Darcy Equation (Table 4.2). The linear trendline passed through the measured

data points was then extrapolated to infinite mean pressure to obtain the equivalent liquid permeability of 156.51 mD (Table 4.2, Figure 4.3). The average gas permeability of the standard (177.75mD) is within the gas permeability range reported for this reference sample (i.e., 162.9 - 183.7 mD) which confirms the reliability of gas permeameter setup as well as the methodology used in this study for direct gas permeability measurement.

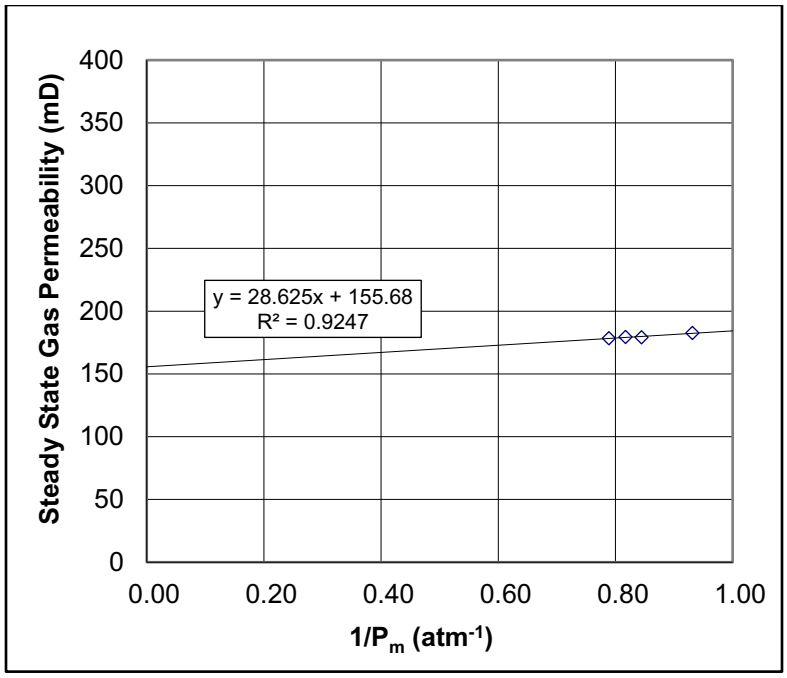

Figure 4.3: Klinkenberg correction for gas permeametry done on reference sample S359

Table 4.2: Gas permeametry results for reference sample S359

Sample Name	Dia (mm)	Length (mm)	Atm. Press. (psi)	Upstream P. (psig)	DP (psi)	Temp. (°C)	Flow rate (cc/min)	K_g (mD)	$1/P_m$ (Abs Atm^{-1})	$(P_1)^2 - (P_2)^2$ $(atm)^2$	Flow rate (cc/s)	Area (cm^2)
Standard S359 (162.9-183.7)	38.10	25.40	14.70	1.03	0.100	21.0	19	182.6	0.937	0.014	0.317	11.4
	38.10	25.40	14.70	2.99	0.580	21.0	107	179.1	0.845	0.093	1.783	11.4
	38.10	25.40	14.70	3.80	1.035	21.0	189	179.4	0.817	0.172	3.150	11.4
	38.10	25.40	14.70	4.74	1.561	21.0	280	178.5	0.788	0.270	4.667	11.4
								k_L =	155.7			

The above analysis was then performed for all 19 samples used in the gas permeametry tests. A sample calculation for permeability using Darcy equation is provided in Appendix A, Sections A.1

and A.2. All the Klinkenberg correction plots are provided in Appendix A, Section A.3. Other data, including sample dimensions, pressures, flow rate, differential and mean pressures etc. are also provided in Appendix A, Section A.3. A summary of the gas permeametry results is presented in Table 4.

Table 4.3: Gas permeametry results

Sample No	Depth (m)	Equivalent liquid permeability obtained using gas permeametry (mD)
SP 1	3959.40 - 3959.79	984.6
SP 3	3961.85 - 3962.32	465.1
SP 4	3967.28 -39 67.98	1744.9
SP 5	3970.33 - 3970.67	3205.9
SP 6	3970.96 - 3971.20	2474.7
SP 7	3973.29 - 3973.58	2203.7
SP 8	3978.57 - 3979.29	859.3
SP 10	4009.40 - 4009.60	212.4
SP 13	4017.54 - 4017.80	386.3
SP 14	4020.98 - 4021.28	241.3
SP 17	4027.94 - 4028.17	225.5
SP 18	4035.83 - 4036.08	1145.0
SP 19	4037.15 - 4037.49	791.8
SP 20	4040.31 - 4040.52	1395.4
SP 22	4043.20 - 4043.39	2170.8
SP 23	4045.73 - 4046.05	3012.7
SP 30	4082.12 - 4082.34	1129.2
SP 31	4083.86 - 4084.10	3955.8
SP 32	4088.01 - 4088.37	1854.3

To check the repeatability of permeability measurements, core plug sample SP 17 was selected for which the gas permeametry measurements were repeated twice. The permeability results for original measurement and replicates for sample SP 17 are shown in Table 4.4. The standard deviation, confidence interval and coefficient of variation (COV) for these measurements are also shown in this Table.

Table 4.4: Repeatability of gas permeability measurements for sample SP 17

Test ID	Klinkenberg-corrected permeability (mD)
SP 17 (original)	214.3
SP 17 1st repeat	244.1
SP 17 2nd repeat	218.2
AVG. (± 2 ST DEV)	225.5 ± 42.1
CONFIDENCE	0.58
COV	0.07

According to Table 4.4, all the permeability measurements are within the range of ±2 ST DEV from the average. The 7% COV shows limited dispersion of the data around the mean. Generally, a COV of less than 10% shows good repeatability of measurements when it comes to the relationship between the standard deviation and mean of the measurement [Feldman, 2018].

5.1.2 Permeability estimation using MIP Data with built-in Katz and Thompson correlation

The MIP test provides porosity, pore size distribution and mercury intrusion pressure versus saturation data for the tested samples. The latter two results can be used to calculate permeability. In this study, Katz and Thompson model [El-Dieb and Hooton 2003] was used to calculate permeability using the MIP data. To check the repeatability of permeability calculations using the mercury intrusion data, the MIP test was repeated twice on sample SP 17 (Table 4.5). The average,

standard deviation, confidence interval and coefficient of variation for these repeats are also included in Table 4.5.

According to Table 4.5, the permeability repeats are within the range of ±2 ST DEV from the average, and the small COV value of 9% shows limited dispersion of the data around the mean, which all show the good repeatability of permeability determination using the MIP data.

For all the other 18 samples, the MIP data was used to calculate permeability using Katz and Thompson model [El-Dieb and Hooton, 2003], and the results are presented in Table 4.6.

Table 4.5: Repeatability of permeability calculations for sample SP 17 based on the MIP data

Sample	Calculated permeability (mD)
SP17	143.1
SP17 1st repeat	170.4
SP17 2nd repeat	150.6
AVG (± 2 ST DEV)	154 ± 28.2
CONFIDENCE	0.51
COV	0.09

Table 4.6: Calculation of permeability using the MIP data

Sample No	K calculated using the MIP data (mD)
SP 1	652.0
SP 3	658.2
SP 4	1747.4
SP 5	2451.2
SP 6	1704.5
SP 7	2072.5
SP 8	495.1
SP 10	181.2
SP 13	353.9
SP 14	359.2
SP 17	154.3
SP 18	753.9
SP 19	618.7
SP 20	1207.5
SP 22	1212.2
SP 23	2867.7
SP 30	605.1
SP 31	3953.6
SP 32	1669.1

5.1.3 Permeability calculation using modified Swanson model based on the MIP data

The modified Swanson correlation [Salimifard et al., 2014] was used to estimate permeability of 19 core plug samples based on the information acquired from their MIP tests. A sample permeability calculation using this method is presented in Appendix B, Section B.1. The

calculations are based on determination of the Swanson parameter for all the tested samples (Appendix B, Section B.2). The permeability results calculated using modified Swanson correlation for these 19 core plug samples are presented in Table 4.7.

Table 4.7: Calculated permeabilities using modified Swanson model based on MIP measurements

Sample No	$(Hg/Pc)_{max}$	K (mD) calculated using Swanson model
SP 1	1.20	543.1
SP 3	1.50	792.0
SP 4	2.01	1299.2
SP 5	2.30	1631.8
SP 6	1.90	1181.3
SP 7	2.20	1513.6
SP 8	0.50	123.6
SP 10	0.59	163.5
SP 13	0.79	267.8
SP 14	0.67	202.7
SP 17	0.40	84.7
SP 18	1.17	520.3
SP 19	1.09	461.6
SP 20	1.21	550.8
SP 22	1.20	543.1
SP 23	1.20	543.1
SP 30	0.90	333.9
SP 31	2.70	2140.0
SP 32	1.90	1181.3

5.2 Comparison of Permeabilities Obtained from Different Methods

The permeability results obtained from different methods are compared in Table 4.8. Considering the gas permeametry method to be the most accurate method (and also the only direct measurement method) in this study, the percentage differences between other methods were calculated against gas permeametry data (Table 4.8).

Table 4.8: Comparison of permeability values obtained from different methods

Sample No	Depth (m)	K (mD)			Relative Difference (%)	
		Modified Swanson Model	Katz and Thompson Model	$K_{L,eq}$ from Gas Permeametry	$(K_{L,eq}-K_{Katz\ \&\ Thompson})/K_{L,eq})\times100$	$(K_{L,eq}-K_{Swanson})/K_{L,eq})\times100$
SP 1	3959.40 - 3959.79	543.1	652.0	984.6	33.8	44.8
SP 3	3961.85 - 3962.32	792.0	658.2	465.1	-41.5	-70.3
SP 4	3967.28 -39 67.98	1299.2	1747.4	1744.9	-0.1	25.5
SP 5	3970.33 - 3970.67	1631.8	2451.2	3205.9	23.5	49.1
SP 6	3970.96 - 3971.20	1181.3	1704.5	2474.7	31.1	52.3
SP 7	3973.29 - 3973.58	1513.6	2072.5	2203.7	6.0	31.3
SP 8	3978.57 - 3979.29	123.6	495.1	859.3	42.4	85.6
SP 10	4009.40 - 4009.60	163.5	181.2	212.4	14.7	23.0
SP 13	4017.54 - 4017.80	267.8	353.9	386.3	8.4	30.7
SP 14	4020.98 - 4021.28	202.7	359.2	241.3	-48.9	16.0
SP 17	4027.94 - 4028.17	84.7	154.3	225.5	31.6	62.4
SP 18	4035.83 - 4036.08	520.3	753.9	1145	34.2	54.6
SP 19	4037.15 - 4037.49	461.6	618.7	791.8	21.9	41.7
SP 20	4040.31 - 4040.52	550.8	1207.5	1395.4	13.5	60.5
SP 22	4043.20 - 4043.39	543.1	1212.2	2170.8	44.2	75.0
SP 23	4045.73 - 4046.05	543.1	2867.7	3012.7	4.8	82.0
SP 30	4082.12 - 4082.34	333.9	605.1	1129.2	46.4	70.4
SP 31	4083.86 - 4084.10	2140.0	3953.6	3955.8	0.1	45.9
SP 32	4088.01 - 4088.37	1181.3	1669.1	1854.3	10.0	36.3

The ranges of variation for permeability values obtained from the modified Swanson model as well as Katz and Thompson model are 84.7–2140.0 mD and 154.3 – 3953.6 mD, respectively, while the direct permeability measurement using gas permeametry resulted in permeability values in the range of 212.4 – 3955.8 mD. The permeability values obtained from the MIP data, using

Katz and Thompson model, seem to be more accurate than the ones obtained based on the mercury intrusion tests but with the application of modified Swanson model. This is also in line with the observations documented in the literature [Rasoul et al, 2019]. In Figures 4.4 and 4.5, the calculated permeability values using Katz and Thompson model as well as modified Swanson model, based on the MIP tests, are plotted versus equivalent liquid permeability, obtained from gas permeametry measurements. These parity plots will help understand the representativeness of any of these two models for permeability estimation when compared to a direct permeability measurement method, and also provide some clarity on whether a correlation could be found in order to correct the estimated permeability values based on comparison against a more accurate direct measurement method. The red dotted lines show the x=y baseline, and the blue dotted lines represent the linear trendlines fitted to the data points. The scatter error associated with these parity plots is visually determined by how the data points spread around the diagonal x=y baseline. Clearly, estimating permeability based on mercury intrusion data has some error when compared to direct gas permeametry; however, the permeability values estimated using built-in correlation associated with the MIP equipment (i.e., Katz and Thompson model) were closer to direct measurements when compared to other employed model that also uses the mercury intrusion data (i.e., modified Swanson model). The built-in Katz and Thompson model in the mercury porosimeter almost always underestimated the permeability values (except only three data points for samples SP 3, SP 4 and SP14). The linear correlation obtained between the Klinkenberg-corrected permeability values and the estimated ones using Katz and Thompson model could be safely used to convert the mercury intrusion permeability estimation to equivalent liquid permeability, considering a slight room for error as depicted in Figure 4.4 from the coefficient of determination value. However for the permeability values estimated using the modified Swanson

model, there is no consistency when it comes to comparison against the direct measurement method, which is evident from the weak linear trend and low coefficient of determination in Figure 4.5.

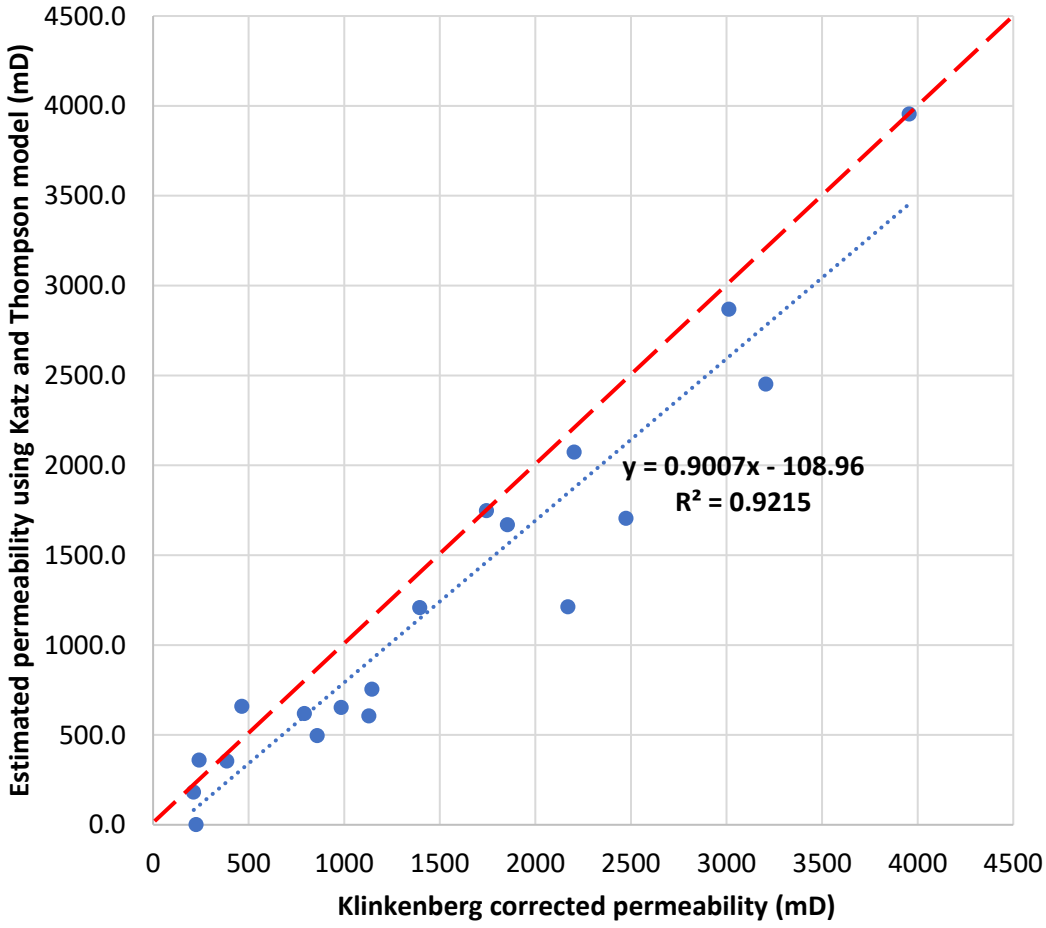

Figure 4.4: Permeability estimation using Katz and Thompson model (from MIP data) vs Klinkenberg corrected permeability

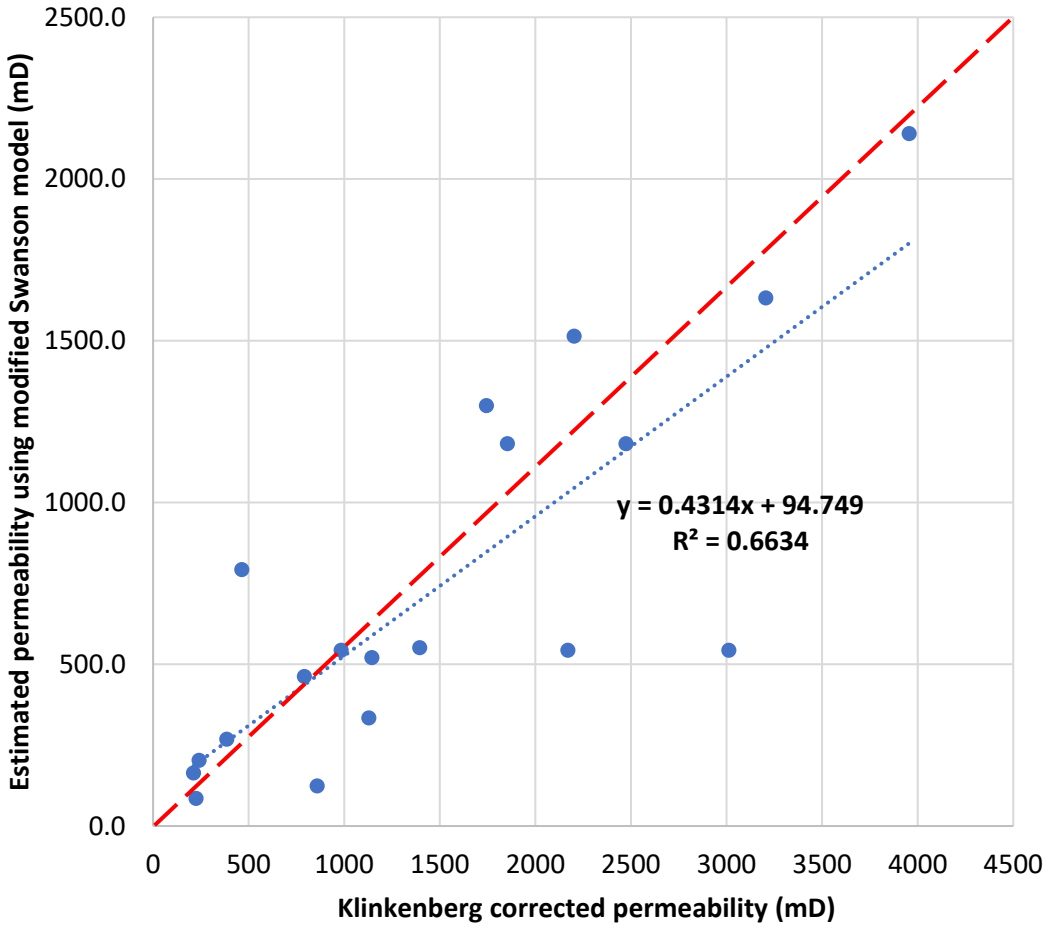

Figure 4.5: Permeability estimation using modified Swanson model (from MIP data) vs Klinkenberg corrected permeability

In Figure 4.6, a pictorial view of comparison between different measured and estimated permeability values is presented. As seen in this histogram, the permeability values estimated using Katz and Thompson model are closer to the directly measured permeability data, but there is significant difference between the permeability data estimated using modified Swanson model when compared to the gas permeametry values.

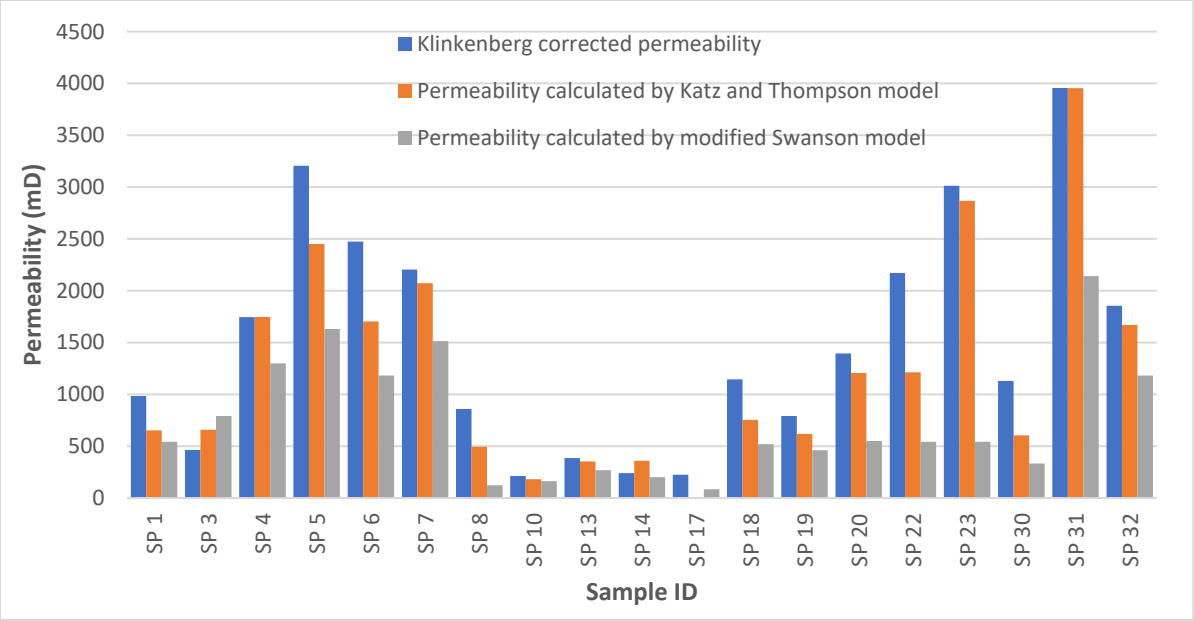

Figure 4.6: The legend in the figure should read: "Klinkenberg corrected permeability" for blue, "Permeability calculated by Katz and Thompson model" for green, and "Permeability calculated by modified Swanson model" for grey

To further assess the generated data statistically, the Bland Altman plot was prepared which shows the 95% limit of agreement for each comparison between the estimation (i.e., predictions using the modified Swanson model in this case) and direct gas permeametry measurements (Figure 4.7). This agreement between the measured and modelled data is graphically presented in the form of ±1.96×ST DEV, meaning that if compared datasets fall within this region on the plot, the methods are comparable, and essentially interchangeable from the statistical perspective. This plot provides information on two compared protocols (i.e., calculated versus measured permeability) to see if they are interchangeable, which is the case when 95% of the data points fall within the allotted interval. The Bland Altman plot for the data points associated with gas permeametry (i.e., measured values) versus Katz and Thompson model (calculated values) is presented in Figure 4.7. Clearly, all but one data points fall within this region, which proves that the calculated permeability

values using Katz and Thompson model based on the MIP data can statistically be used instead of direct permeametry measurements within 95% of accuracy.

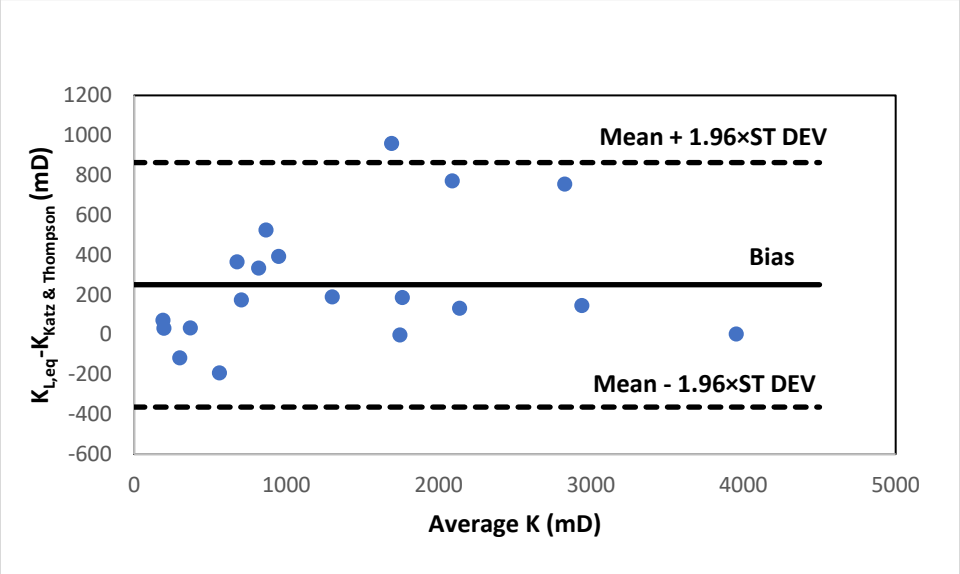

Figure 4.7: Bland–Altman plot for two permeability determination methods of gas permeametry (direct measurement method) and mercury intrusion (estimation method)

The same plot was done for permeability of gas permeametry and modified Swanson model as shown in Figure 4.8.

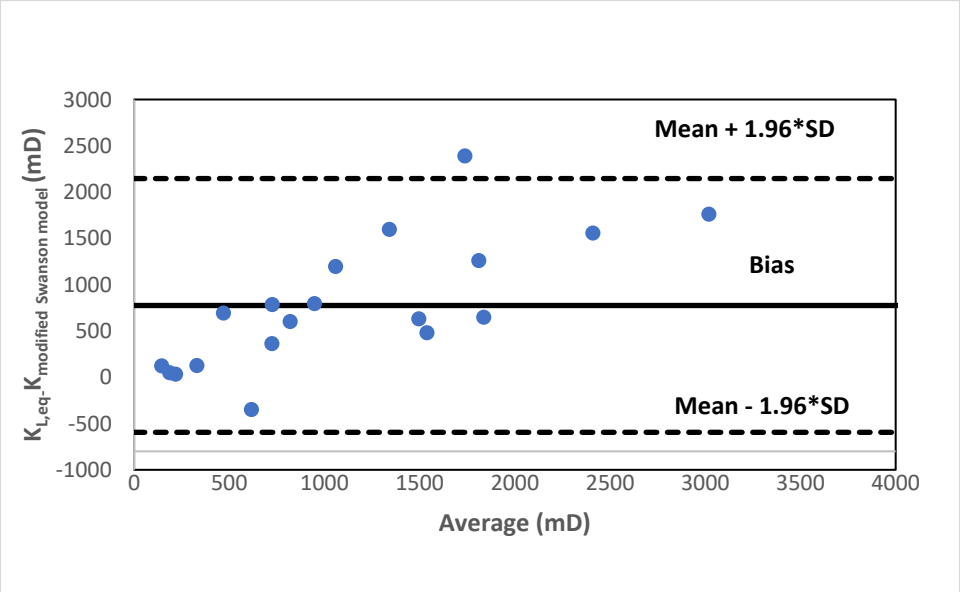

Figure 4.8: Bland–Altman plot for two permeability determination methods of gas permeametry (direct measurement method) and modified Swanson model (estimation method)

Although more than 95% of the data points falls within the limits of ±1.96×ST DEV but due to the much difference between the data of the two methods, the bias and the limits are higher than those of the previous chart in Figure 4.7.

5.3 Determination of Core Plug Porosities

The core plug porosities were measured using the MIP method in this study. Details of the measurement procedure were discussed in Section 2.2.1.1. The equipment was first calibrated using a Silica Alumina standard sample labeled 004/16822/00 REF MAT. The porosity measurement reliability was confirmed by testing this standard material. Once the measurement reliability and equipment calibration were confirmed, the MIP tests were conducted on small segments cut out from each core plug sample. In order to test the repeatability of measurements, the mercury intrusion process was done on three small segments cut out from samples SP3. The repeatability analysis was performed by calculating some statistical measures (i.e., average, standard deviation, confidence interval, and coefficient of variation). For the same depths of interest, the porosity values measured using helium pycnometry method were also extracted from the literature (Core Laboratories, 1999) for comparison purposes against porosities measured in this study using the MIP method. From the MIP tests in this study, several other parameters were also extracted including median pore diameter, total pore area, total intrusion volume, average pore diameter, bulk density and skeleton density; however, only porosity and permeability data were discussed in this thesis to focus on the intended objectives.

5.3.1 Core plug porosimetry using helium pycnometry – literature data

The porosity was analysed by Core Laboratories Inc. using helium pycnometry method. The results are presented in Table 4.9.

5.3.2 Porosity measurement using MIP test

The standard Silica Alumina sample, labeled as 004/16822/00 REF MAT, was analyzed using 9500 Autopore Porosimeter. In Table 4.10, the measured total intruded mercury volume as well as median pore diameter for the standard sample are reported, which are within the acceptable range documented for the Silica Alumina material. This shows the reliability of measurement protocol and proves the validity of equipment calibration.

In order to further assess the reliability of MIP measurements, the porosity measurements were repeated three times for SP 3 sample. Some statistical parameters including average, standard deviation, confidence interval, and coefficient of variation. The repeated porosity measurements were in ±2 ST DEV from the average, and the very low COV of 3.8% proves that the repeated measurements had limited dispersion around the mean porosity value. These statistical parameters verify the repeatability of porosity measurements when similar testing protocol and equipment type were used (Table 4.11). When accuracy of testing protocol, reliability of the equipment, and repeatability of the measurements were validated, small sub-samples were cut out from each of the 19 core plug samples to be used for the MIP tests. The results are shown in Table 4.12.

Table 4.9: Core plug porosities from helium pycnometry - literature data

Sample No	Depth (m)	Porosity from helium pycnometry measurement [Core Laboratories, 1999]
SP 1	3959.40 - 3959.79	18.8
SP 3	3961.85 - 3962.32	21.6
SP 4	3967.28 -3967.98	7.4
SP 5	3970.33 - 3970.67	22.0
SP 6	3970.96 - 3971.20	21.3
SP 7	3973.29 - 3973.58	21.9
SP 8	3978.57 - 3979.29	20.5
SP 10	4009.40 - 4009.60	16.1
SP 13	4017.54 - 4017.80	24.6
SP 14	4020.98 - 4021.28	19.1
SP 17	4027.94 - 4028.17	12.2
SP 18	4035.83 - 4036.08	19.7
SP 19	4037.15 - 4037.49	20.2
SP 20	4040.31 - 4040.52	19.0
SP 22	4043.20 - 4043.39	19.5
SP 23	4045.73 - 4046.05	21.6
SP 30	4082.12 - 4082.34	17.9
SP 31	4083.86 - 4084.10	21.0
SP 32	4088.01 - 4088.37	20.3

Table 4.10: Mercury intrusion test performed on Silica Alumina standard

Parameter	Calibration range for standard	Measured values
Total intrusion volume (mg/g)	0.50 - 0.54	0.5295
Median pore diameter (μm)	0.0064 - 0.0074	0.0068

Table 4.11: Porosity measurement repeatability for SP 3 sample using the MIP method

Test ID	Porosity (%)
SP 3 original test	20.6
SP 3 1st repeat	20.6
SP 3 2nd repeat	22.0
AVG (± 2 ST DEV)	21.1 ± 1.6%
CONFIDENCE	0.029
COV	0.038

Table 4.12: Core plug porosity using mercury intrusion

Sample ID	Depth (m)	Porosity using the MIP method (%)
SP 1	3959.40 - 3959.79	19.2
SP 3	3961.85 - 3962.32	20.6
SP 4	3967.28 -3967.98	22.0
SP 5	3970.33 - 3970.67	19.0
SP 6	3970.96 - 3971.20	20.3
SP 7	3973.29 - 3973.58	20.5
SP 8	3978.57 - 3979.29	17.9
SP 10	4009.40 - 4009.60	14.3
SP 13	4017.54 - 4017.80	18.3
SP 14	4020.98 - 4021.28	17.6
SP 17	4027.94 - 4028.17	11.4
SP 18	4035.83 - 4036.08	18.1
SP 19	4037.15 - 4037.49	17.9
SP 20	4040.31 - 4040.52	17.9
SP 22	4043.20 - 4043.39	18.0
SP 23	4045.73 - 4046.05	20.0
SP 30	4082.12 - 4082.34	15.7
SP 31	4083.86 - 4084.10	18.8
SP 32	4088.01 - 4088.37	20.5

5.4 Comparison of Porosities Obtained Using Different Methods

The porosity results for 19 core plug samples, measured using two methods of helium pycnometry and mercury porosimetry, along with calculated relative difference in percentage are presented in Table 4.13.

Table 4.13: Comparison of porosity values obtained from different methods

Sample ID	Porosity from helium pycnometry [Core Laboratories, 1999]	Porosity from MIP (%)	Relative difference (%) $\left[\frac{\varphi_{Helium\ Pycnometry} - \varphi_{MIP}}{\varphi_{Helium\ Pycnometry}}) \times 100\right]$
SP 1	18.8	19.2	-2.1
SP 3	21.6	20.6	4.6
SP 4	7.4	22.0	-197.3
SP 5	22.0	19.0	13.6
SP 6	21.3	20.3	4.7
SP 7	21.9	20.5	6.4
SP 8	20.5	17.9	12.7
SP 10	16.1	14.3	11.2
SP 13	24.6	18.3	25.6
SP 14	19.1	17.6	7.9
SP 17	12.2	11.4	6.6
SP 18	19.7	18.1	8.1
SP 19	20.2	17.9	11.4
SP 20	19.0	17.9	5.8
SP 22	19.5	18.0	7.7
SP 23	21.6	20	7.4
SP 30	17.9	15.7	12.3
SP 31	21	18.8	10.5
SP 32	20.3	20.5	-1.0

For most of the samples tested in this study, helium pycnometry method provides greater porosity values than those obtained from the mercury intrusion method. This is in agreement with observations from the literature [Mastalerz et al., 2013]. The porosity values obtained from the helium pycnometry range from 7.4% to 24.6% while those measured with mercury intrusion range from 11.4% to 22.0%. These samples all have high porosity values, which is in agreement with their sandstone lithology. In Figure 4.9, the porosity values from helium pycnometry are plotted versus those from the MIP test. There is a weak correlation between the porosity values from these two methods, and the data spread around the red dotted line of x=y shows the scatter error associated with the porosity measurement.

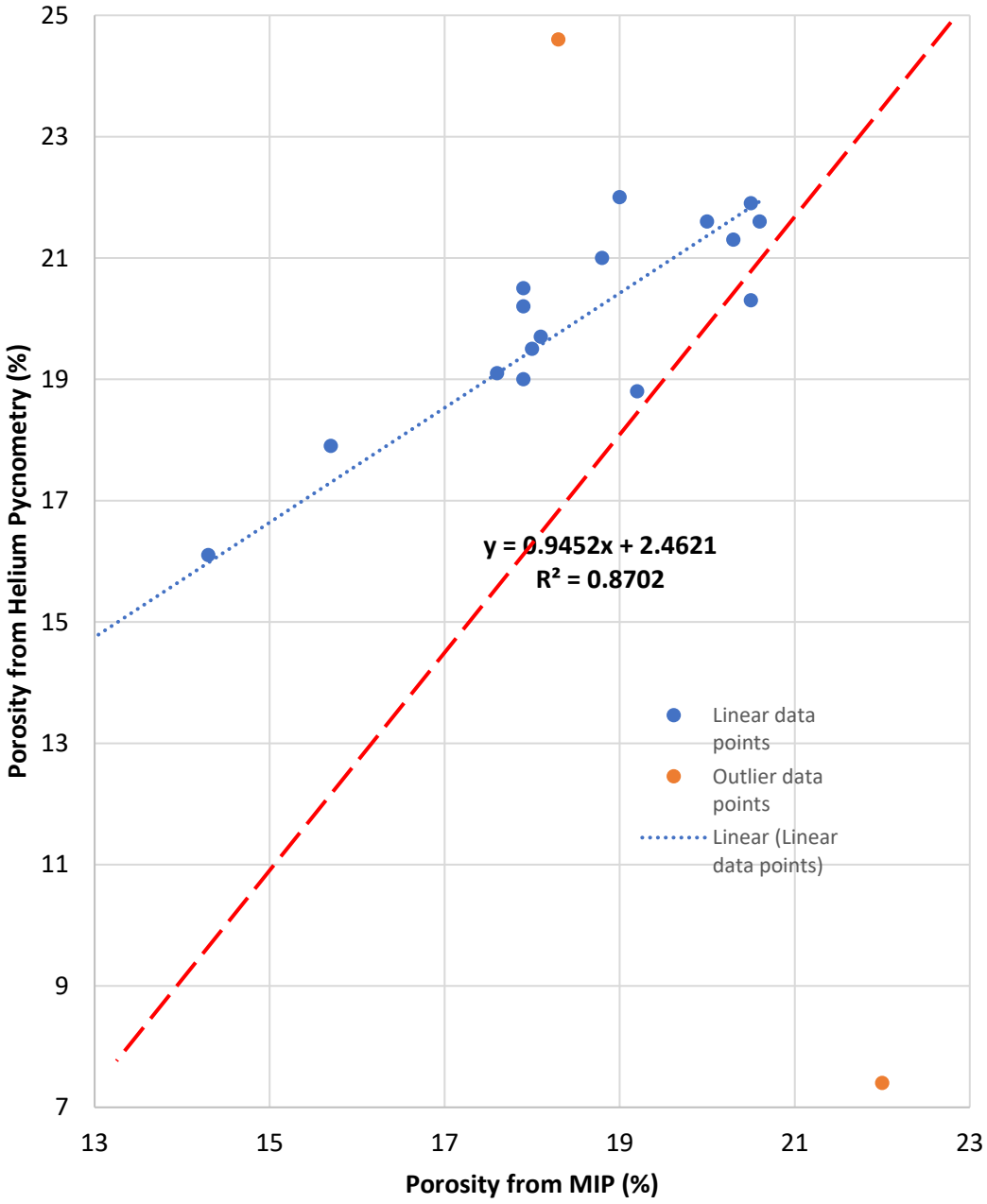

Figure 4.9: Parity plot of porosity values measured using helium pycnometry vs. those from mercury intrusion

Although most of the results from both methods were close to each other but few samples had higher deviations such the SP 4 and SP 13. This resulted in a low R^2 value. However, if we do not consider these two data points in the linear trend fitting as done in this plot, a much better

correlation was obtained. The two points not considered are indicated in red marker. Considering the overall agreement between the majority of the samples, this correlation can be useful in adjusting the MIP porosity closer to the helium pycnometry equivalent. The graphical illustration of the comparison between the porosity results is shown in a histogram in Figure 4.10.

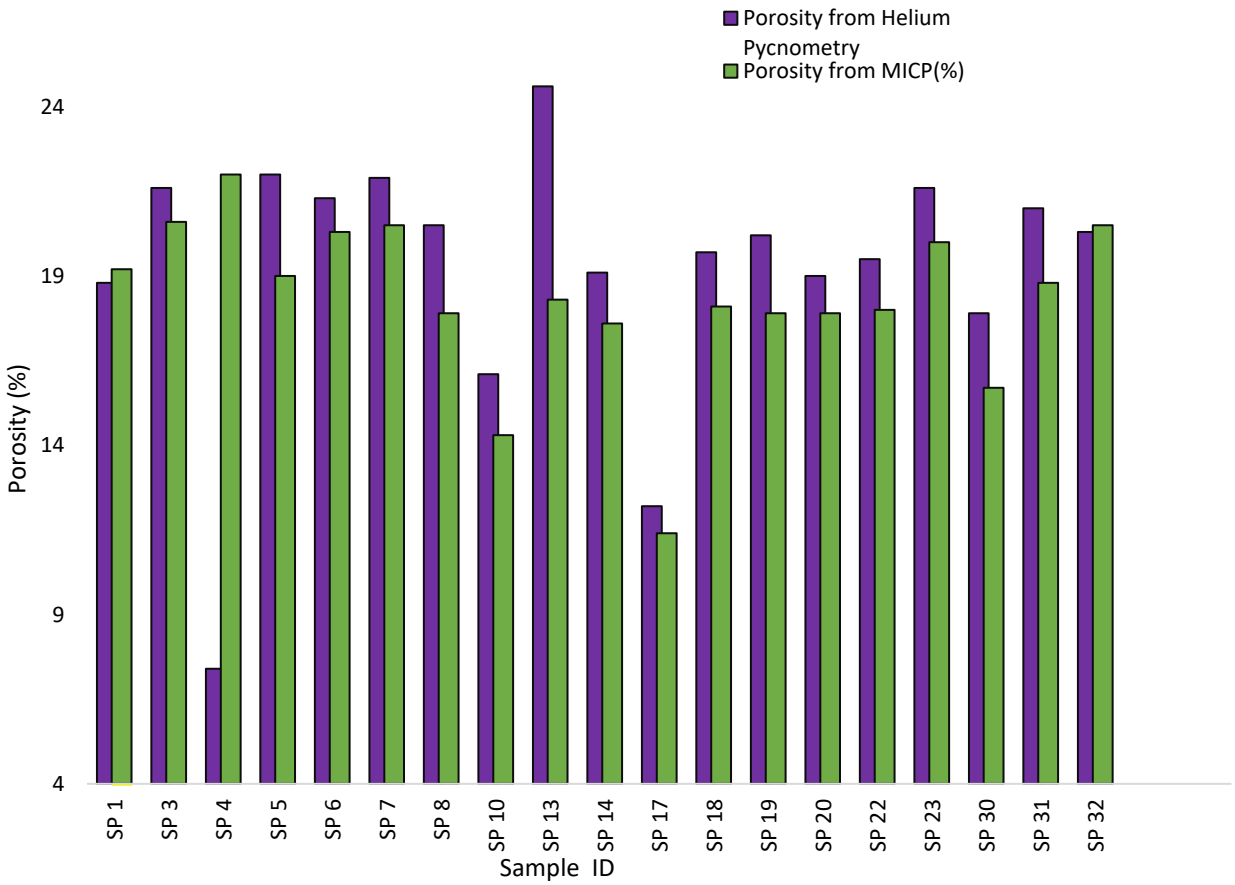

Figure 4.10: Porosity from helium pycnometry for purple and Porosity from MIP for green.

In Figure 4.10, the porosity values from helium pycnometry are generally greater than those from the MIP method. We assume the helium pycnometry method to be a more accurate and representative porosity measurement method compared to the MIP method because of the representativeness of tested sample (i.e., whole sample for helium pycnometry versus a small cutout in MIP), non-destructive nature of gas vs. mercury in damaging the pore structure, and the ease/possibility of measurement repeat on the same sample (not possible for MIP). Therefore, it is

attempted to see how close the MIP measurements could be to the more accurate and representative helium pycnometry data. In Figure 4.11, the Bland Altman plot is presented for the MIP porosity values versus the helium pycnometer data to statistically assess their comparison and see if these two measurements are interchangeable by looking into the data point population within the ±1.96×ST DEV region from the mean, which is equivalent to 95% agreement between the two methods. Most of the data points on Figure 4.11 fall within this region, which proves that the MIP method can be statistically used as a replacement for the helium pycnometry method for porosity measurement within 95% accuracy. Two of the samples SP 4 and SP 13 that has a higher difference are coloured in red while the others are in blue.

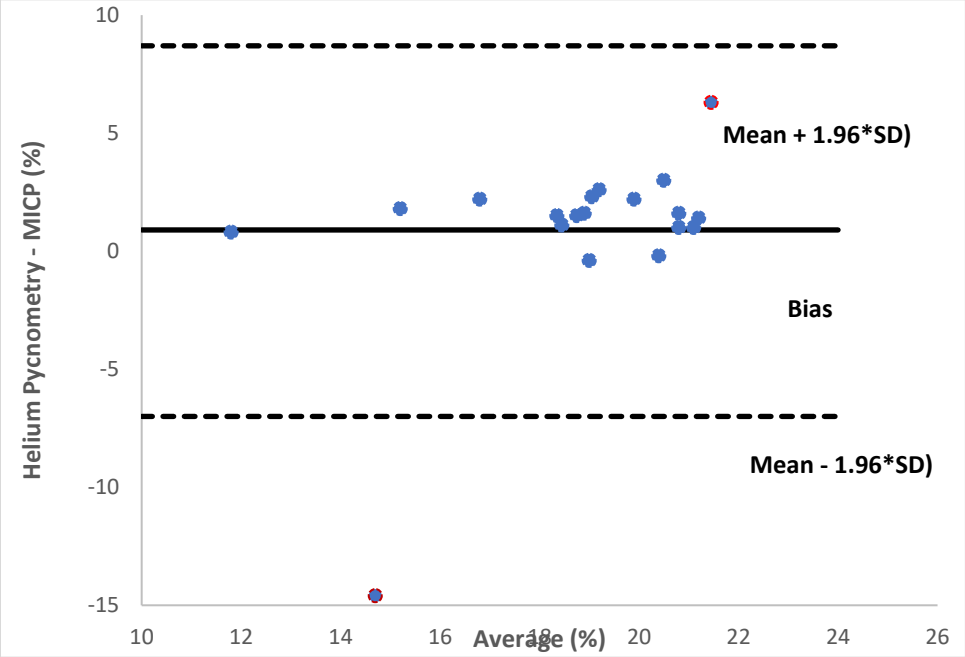

Figure 4.11: Bland–Altman plot for two porosity measurement methods of helium pycnometry and mercury intrusion

5.5 Sources of Error

There are outliers in all measured porosity and permeability values. For permeability and porosity measurements, Klinkenberg corrected air permeametry and helium pycnometry were considered as the baseline methods, respectively, for relative difference calculations. There are some outliers in the measured data, resulted in poor agreement between methods and abnormal trends seen in the literature [Rasoul et al, 2019], which have been highlighted throughout the thesis for the traceability purposes. There are possible root causes for these outliers, including errors in sampling, labelling, non-representativeness of the sub-samples taken out, and equipment-related issues such as drifting off the calibration. Unfortunately, most of those samples are no longer available for repeated testing, but when the sample was already at hand, measurements were repeated. It is believed that these limited uncertain measurements do not negatively impact the general trends since they constitute only a small portion of measurements reported in this thesis. Therefore, the generalization statements included in this thesis are acceptable.

Chapter 6: Conclusion

Depending on the level of accuracy needed for the test, the permeability and porosity results from 9500 Autpore IV Porosimeter can be useful while considering the level of deviation from values obtained by other methods. The porosity and permeability results from the MIP test can be improved by applying the correction correlations proposed in this thesis to obtain more accurate results, comparable to the data obtained using more reliable measurement methods. This research work proposes correction correlations to modify data acquired from 9500 Autpore IV Porosimeter. Through this correction effort, more representative porosity and permeability values will be obtained based on mercury intrusion porosimetry. The proposed correction correlations are only applicable to sandstone samples; therefore, future research could be focused on developing the same for other rock types such as dolomite, limestone etc. In addition, more accurate MIP measurements could be done by selecting more representative rock samples, preferably the full diameter thin sections with the aid of proper penetrometer sizes. Other limitation is the non availability of the Pycnometer to directly measure the porosity instead of using data from literature. Also having more sample number could generate a more representative correlations. This research could be improved on by carrying out the test of both porosity and permeability on the same sample. This can be done by first carrying out the gas permeameter and pycnometry test before using same sample for MIP using a larger penetrometer. This will reduce some errors.

Reference

Adams, A. J. (2005) Relationship Between Observed Pore and Pore-Throat Geometries Measured Porosity and permeability, and Indirect Measure of Pore Volume by Nuclear Magnetic Resonance. pp 72-74.

Al-Bulushi, N. I., Kraishan, G. and Hursan, G. (2019) Capillary Pressure Corrections, Quality Control and Curve Fitting Workflow, European Association of Geoscientists & Engineers, 11th International Petroleum Technology Conference, p. 3.

Alton, A. B. (2015) Interpreting Permeability from Mercury Injection Capillary Pressure Data, *AAPG Annual Convention and Exhibition*.

Anderson, W. G. (1986) Wettability Literature Survey- Part 1: Rock/Oil/Brine Interactions and the Effects of Core Handling on Wettability, *J Pet Technol* 38 (10): 1125–1144, Paper Number: SPE-13932-PA, https://doi.org/10.2118/13932-PA.

Anton Parr. (n.d) Mercury Intrusion Porosimetry Basics: Measuring Pores in Solid, https://wiki.anton-paar.com/en/mercury-intrusion-porosimetry-basics-measuring-pores-in-solids/, Accessed 14 October 2022.

Apisaksirikul, S. and Blasingame, T.A. (2016) The Development and Application of a New Semi-Analytical Model to Estimate Permeability from Mercury Injection Capillary Pressure, *Unconventional Resources Technology Conference,* URTeC: 2460639, San Antonio, TX, USA.

Arabjamaloei, R., Daniels, D., Ebeltoft, E., Petersen, E., Pitman, J. R. and Ruth, D. (2019) Validation of Permeability and Relative Permeability Data Using Mercury Injection Capillary Pressure Data, Presented at the International Symposium of the Society of Core Analysts in Trondheim, Norway, 27-30, SCA2018-002, https://doi.org/10.1051/e3sconf/20198901001.

Babak, S., Ruth, D. W., Green, D., and Dragan, V. (2014) Developing a Model to Estimate Permeability from other Petrophysical Data, *International Symposium of the Society of Core Analysts* held in Avignon, France.

Brace, W.F., Walsh, J.B., Frangos, W.T. (1968). Permeability of granite under high pressure. J. Geophys. Res. 73, 2225–2236. https://doi.org/10.1029/ JB073i006p02225.

Bruce, W. and Welge, H. J. (1947) The Restored-State Method for Determination of Oil in Place and Connate Water, *Drilling and Production Practice*.

Champion, C. F. and Davy, N. (1937) Properties of Matter, New York Prentice Hal1, pp 99-10, 1937.

Choquette, P. W., and Pray L. C. (1970) Geological nomenclature and classification of porosity in sedimentary carbonates: AAPG Bulletin, v. 54, p. 207–250.

Core Laboratories (1999) HMDC B16-17 Core Analysis Result, *CNLOPB Offshore Petroleum Board Data Information Hub*, hibernia-b-16-17 | C-NLOPB Online Portal (arcgis.com), Accessed date: 12-06-2021.

Engineering ToolBox (2014) Gases-Dynamic Viscosities, https://www.engineeringtoolbox.com/gases-absolute-dynamic-viscosity-d_1888.html, Accessed: 12/03/2022.

Engineering ToolBox (2014) Gases-Dynamic Viscosities. DOI: https://www.engineeringtoolbox.com/gases-absolute-dynamic-viscosity-d_1888.html, Accessed: 12/03/2022

Donaldson, E. C., Ewall, N., Baljit S. (1967) Characteristics of Capillary Pressure Curves, Journal of Petroleum Science and Engineering, https://doi.org/10.1016/0920-4105(91)90017.

El-Dieb A.S, Hooton R.D. (2003) Evaluation of the Katz-Thompson model for estimating the water permeability of cement-based materials from mercury intrusion porosimetry data, *Sciencedirect.*

Giavarine, D. (2015) Understanding Bland Altman Analysis, *Croatian Society for Medical Biochemistry and Laboratory Medicine*, DOI: 10.11613/BM.2015.015.

Glover, P.W.J. (2010) Formation Evaluation, KUPDF publication, pp 48-53, https://kupdf.net/download/formation-evaluation-msc-course-notes-paul-glover_58ba5d5de12e890933add375_pdf.

Guo, B.Y., Ghalambor, A., Duan, S.K. (2004) Correlation between sandstone permeability and capillary pressure curves, J. Petrol. Sci. Eng. 43 (2), 239–246.

Griese. E. W. Jr. (n.d) Adhesion Factors of Surface Energy and Surface Tension, Get Tech Talk Newsletter, https://corkindustries.com/adhesion-factors-of-surface-energy-surface-tension.

Feldman F. (2018). Coefficient of Variation, Isixsigma publication, Doi: Coefficient of Variation - isixsigma.com.

Feisheng, F., Wang, P., Wei, Z., Jang, G., Xu, D. and Zhang, J. (2020) A New Method for Predicting the Permeability of Sandstone in Deep Reservoirs. Geofluids, vol. 2020, Article ID 8844464, 16 pages, https://doi.org/10.1155/2020/8844464.

Fleury, M., Poulain, P., Ringot, G. (2001) Positive Imbibition Capillary Pressure Curves Using the Centrifuge Technique. *Petrophysics* 42 (04).

Fricke, H. (1924). A Mathematical Treatment of the Electric Conductivity and Capacity of Disperse Systems I, The Electric Conductivity of a Suspension of Homogeneous Spheroids. *Physical Review*, vol. 24, no. 5, pp. 575-587.

Giavarine, D. (2015). Understanding Bland Altman Analysis. *Croatian Society for Medical Biochemistry and Laboratory Medicine*, doi: 10.11613/BM.2015.015.

Hasan, A. N., Anifowose, F. and Abdulraheem, A. (2013). Applying Artificial Intelligence Techniques to Develop Permeability Predictive Models using Mercury Injection Capillary-Pressure Data. King Fahd University of Petroleum & Minerals, *SPE* 168109, https://doi.org/10.2118/168109-MS.

Haugen, H.J. & Bertoldi, S. 2017 Characterization of morphology-3D and porous structure 27 29 Tanzi, M.C. & Fare, S. *Characterization of polymeric biomaterials.* Woodhead Publishing Cambridge, MA https://doi.org/10.1016/B978-0-08-100737-2.00002-9.

Honarpour, M., Koederitz, L., and Harvey, A. H. (1986). Relative Permeability of Petroleum Reservoirs, Boca Raton, Florida USA: CRC.

Ismael H. F, Jacobo C. (2013) Techniques for rock permeability determination II. The pore pressure oscillation method, Research gate, http://dx.doi.org/10.13140/RG.2.1.4493.7208

Jang, J. Z. S., and Santamarina, J.C. (2016). Capillary pressure across a pore throat in the presence of surfactants. Water Resources, 52, 9586–9599, doi:10.1002/2015WR018499.

Jarrahi, M., Ruth, W. D., Bassuoni, M. T. and Holländer, H. M. (2019) Porosity Measurement of Low Permeable Materials Using Gas Expansion Induced Water Intrusion Porosimetry, GEIWI Scientific Reports, Vol. 9, Article number: 17554.

Jouniaux, L., S. Lallemant and Pozzi, J.-P. (1994). Changes in the permeability, streaming potential and resistivity of a claystone from the Nankai prism under stress, Geophys. Res. Lett., 21, 149-152.

Katz, A. J. and Thompson, A. H. (1987) Prediction of rock electrical conductivity from mercury injection measurements, *Journal of Geophysical Research*, Vol. 92, No. B1, pp. 599-607.

Kunash Instruments Pvt Ltd. (n.d) Autopore – Model iv Series – 9500 Mercury Intrusion Porosimetry. https://www.environmental-expert.com/products/autopore-model-iv-series-9500-and-9510-mercury-intrusion-porosimeter-607313

Leon y Leon, C.A. (1998) A new perspectives in mercury porosimetry, Advanced interface science, https://doi.org/10.1016/S0001-8686(98)00052-9.

Leverett, M.C. (1941) Capillary Behavior in Porous Solids, Transactions of AIME, Vol. 142, pp. 152-169.

Liu, J.Q., Zhang, C.M., Zhang, Z.S. (2016) Combine the capillary pressure curve data with the porosity to improve the prediction precision of permeability of sandstone reservoir, J. Petrol. Sci. Eng. 139, 43–48.

Mahmound, J., Mehran, S., Mohammed, T. (2007) Estimation of Saturation Height Function Using Capillary Pressure by Different Approaches, *EUROPEC/EAGE Conference and Exhibition*, London, U.K. Paper Number: SPE-107142-MS, https://doi.org/10.2118/107142-MS.

Mastalerz M, Schimmelmann A, Drobniak A. Chen Y. (2013) Porosity of Devonian and Mississippian New Albany Shale across a maturation gradient: Insights from organic petrology, gas adsorption, and mercury intrusion, *AAPG Bulletin 97(10):1621-1643,* DOI: 10.1306/04011312194.

McDonald, A. (2020) Porosity-Permeability Relationships Using Linear Regression in Python. *Towards Data Science*, https://towardsdatascience.com/porosity-permeability-relationships-using-linear-regression-in-python-eef406dc6997.

McPhee, C., Reed, J. and Zubizarreta, I. (2015) Best Practice in Coring and Core Analysis. 1st Edition, Chapter 1 and 9, https://doi.org/10.1016/B978-0-444-63533-4.00001-9. https://doi.org/10.1016/B978-0-444-63533-4.00009-3.

Melrose, J. C. (1988) Use of Water-Vapor Desorption Data in the Determination of Capillary Pressures at Low Water Saturations, *SPE* Res Eng 3 (03): 913–918.

Metwally Y. M, Sondergeld C. (2011) Measuring low permeabilities of gas-sands and shales using a pressure transmission technique, International Journal of Rock Mechanics and Mining Sciences, 48(7):1135-1144.

Merlin Powder Characterization. (n.d) True Density & Helium Pycnometry, True Density | Gas Pycnometry and Helium Pycnometry | Merlin PC (merlin-pc.com), Accessed date: 03/04 2021.

Pal, A., Garia, S., Karangat, R. and Nair, A. (2018) Porosity Estimation by Digital Image Analysis, ONGC Bulletin 53. 59-72

Paul W. J. G. (2010) Formation Evaluation, MSc Course Note, Department of Geology and Petroleum Geology, University of Aberdeen, KUPDF publication, pp 48 – 53, 2010. [https://kupdf.net/download/formation-evaluation-msc-course-notes-paul-glover_58ba5d5de12e890933add375_pdf.

Perm TIPM Laboratory. (2018) Fundamentals of Fluid Flow in Porous Media, Chapter 2**.**

Penumadu, D. and Dean, J. (2000) Compressibility effect in evaluating the pore-size distribution of kaolin clay using mercury intrusion porosimetry. *Canadian Geotechnical Journal.*

Petroshine, (n.d) Porosity Measurement, Porosity Measurement | Petro Shine.

Pittman, E. D. (1979) Porosity, diagenesis, and productive capability of sandstone reservoirs, in P. A. Scholle, and P. R. Schluger, eds., Aspects of Diagenesis: Society Economic Paleontologists and Mineralogists Special Publication 26, p. 159–173.

Purcell, W. R. (1949) Capillary Pressures - Their Measurement Using Mercury and the Calculation of Permeability Therefrom. *Journal of Petroleum Technology*, Vol. 1, No. 02.

Rezaee, R., Saeedi, A., Clennell, B. (2012) Tight gas sands permeability estimation from mercury injection capillary pressure and nuclear magnetic resonance data. J. Petrol. Sci. Eng. 88, 92–99.

Ritter, H. L. and Drake, L. C, Z. (1945) Pressure Porosimeter and Determination of Complete Macropore-Size Distributions Ind. Eng. Chem. Anal. Ed. 1945, 17, 12, 782–786, https://doi.org/10.1021/i560148a013.

Rouquerol, J., Baron, G. R., Denoyel, Giesche H., Groen, J., Klobes, P., Levitz, P., Neimark, A. V., Rigby, R., Skudas, R., Sing, K., Thommes, M. and Unger, K. (2011) Liquid intrusion and alternative methods for the characterization of macroporous materials, IUPAC Technical Report, Pure Appl. Chem., Vol. 84, No. 1, pp. 107–136. https://doi.org/10.1351/PAC-REP-10-11-19.

Saki, M., Siahpoush, S. and Khaz'ali, A.R. (2020) A new generalized equation for estimation of sandstone and carbonate permeability from mercury intrusion porosimetry data, *J Petrol Explor Prod Technol* 10, 2637–2644, https://doi.org/10.1007/s13202-020-00900-w.

Shafer, J. & Neasham, J. (2000) Application of mercury injection capillary pressure to mudrocks: Conformance and compression corrections, International Symposium of the Society of Core Analysts, SCA, Retrieved from http://www.ux.uis.no/~s-skj/ipt/Proceedings/SCA.1987-2004/1981-SCA2000-1921.pdf.

Swanson B. (1981) A Simple Correlation between Permeability and Mercury Capillary Pressures, *Journal of Petroleum Technology*, Vol. 33, No. 12, pp. 2488-2504.

Thomeer, J. H. (1960) Introduction of a Pore Geometrical Factor Defined by the Capillary Pressure Curve, *Journal of Petroleum Technology,* Vol. 12, No. 13.

Thompson, A.H. and Raschke, R. A. (1987) Estimation of Absolute Permeability from Capillary Pressure Measurements, *SPE Annual Technical Conference and Exhibition*, Dallas, Texas, S.

Thomson, W. (Lord Kelvin) (1870) On the Equilibrium of Vapour at a Curved Surface of Liquid, Proc, Roy. Soc. Edinburgh, 7, 63–67; Phil. Mag. (1871) 42, Ser. 4, 448-452, https://doi.org/10.1080/14786447108640606.

Rasoul D, Einar E, Richard J. D. (2019) Validation of Permeability and Relative Permeability Data Using Mercury Injection Capillary Pressure Data, E3S Web of Conferences 89, 01001.

Rezaee, R., Saeedi, A., Clennell, B. (2012) Tight gas sands permeability estimation from mercury injection capillary pressure and nuclear magnetic resonance data. J. Petrol. Sci. Eng. 88, 92–99.

Washburn, E. W. (1921). The Dynamics of Capillary Flow. *The Physical Review*, Vol. 17, No. 03, pp. 273-283.

Waszkiewicz, S., Krakowska-Madejska, P. & Puskarczyk, E. (2019) Estimation of absolute permeability using artificial neural networks (multilayer perceptrons) based on well logs and laboratory data from Silurian and Ordovician deposits in SE Poland. *Acta Geophys.* 67, 1885–1894. https://doi.org/10.1007/s11600-019-00347-6.

Wells, J. D. and Amaefule, J. O. (1985) Capillary Pressure and Permeability Relationships in Tight Gas Sands, SPE/DOE Low Permeability Gas Reservoirs Symposium, Denver, Colorado.

Wong S. (2017) A review of contact angle techniques, Contact Lens Update.

Xiao, L., Xiao-Peng, L., Chang-Chun, Z., Xiao-Xin, H., Zhi-Qiang, M., Yu-Jiang, S., Hao-Peng, G. and Gao-Ren, L. (2014) Comparative Study of Models for Predicting Permeability from

Nuclear Magnetic Resonance (NMR) Logs in Two Chinese Tight Sandstone Reservoirs, Acta Geophysica, Vol. 62, No. 1, pp. 116-141 DOI: 10.2478/s11600-013-0165-6.

Appendix

A. Gas Permeametry

A.1- Formula, parameters and definition of units for permeability calculation using gas permeametry data:

The Darcy equation is expressed below for steady state gas permeability is given as:

$$k = 2000Q\mu LP_1/A(P_1^2 - P_2^2)$$

$$P_2 = P_1 - DP$$

$$Pm = (P_1 + P_2)/2$$

P_1 is the inlet pressure (psig)

P_2 is the outlet pressure (psig)

P_m is the mean pressure (psig)

DP is the pressure difference (psi)

L is the length of the sample (cm)

D is the diameter of the sample (cm)

μ is the viscosity of nitrogen (cp)

A is the area (cm^2)

A.2- Calculation example: Gas permeability of SP 13 sample

$$Area\ (A) = \pi r^2, Flowrate\ (cc/sec) = cc/min * 0.0166667$$

$$Absolute\ pressure\ (psia) = guage\ pressure\ (psig) + 14.696\ psi$$

$$Pressure\ (atm) = pressure\ (psia)/14.6959$$

$$Viscosity\ of\ nitrogen\ at\ test\ operating\ temperature\ =\ 0.01747965cp\ (20^0C)$$

$diameter\ =\ 3.5\ cm,$

$P_1 =\ 0.467\ psig$

$Temp.\ =\ 20.0\ °C$

$Length\ =\ 4.4\ cm,$

$DP\ =\ 0.114\ psia$

$\mu\ =\ 0.01747965\ cP\ [Engineering\ Tool\ Box, 2014]$

$Q\ =\ 27.00\ cc/min\ =\ 27 \times\ 0.016667\ =\ 0.4500\ cc/sec$

$Area\ = \pi(3.5/2)2\ =\ 9.62\ cm^2$

$$P1\ (atm)\ = \frac{(0.467 + 14.6959)}{14.696} =\ 1.0318\ atm$$

$$DP\ (atm)\ = \frac{0.114}{14.696} =\ 0.00776atm, \qquad P2(atm) = 1.0318\ - 0.00776 =\ 1.0240\ atm$$

$$Pm\ (atm)\ = \frac{(1.0318 + 1.0240)}{2} =\ 1.0279\ atm,$$

$1/Pm\ (\text{atm}^{-1})\ =\ 1/1.0279\ =\ 0.9729\ \text{atm}^{-1}$

$(P_1)^2 - (P_2)^2 = 1.0318^2 - 1.024^2 = 0.016035$

$$k\ =\ 2000 \times 0.45 \times 0.01747965 \times 1.0318 \times \frac{4.4}{0.016035 \times 9.62} =\ 463.0\ mD$$

A.3- Plots illustrating Klinkenberg correction for gas permeability

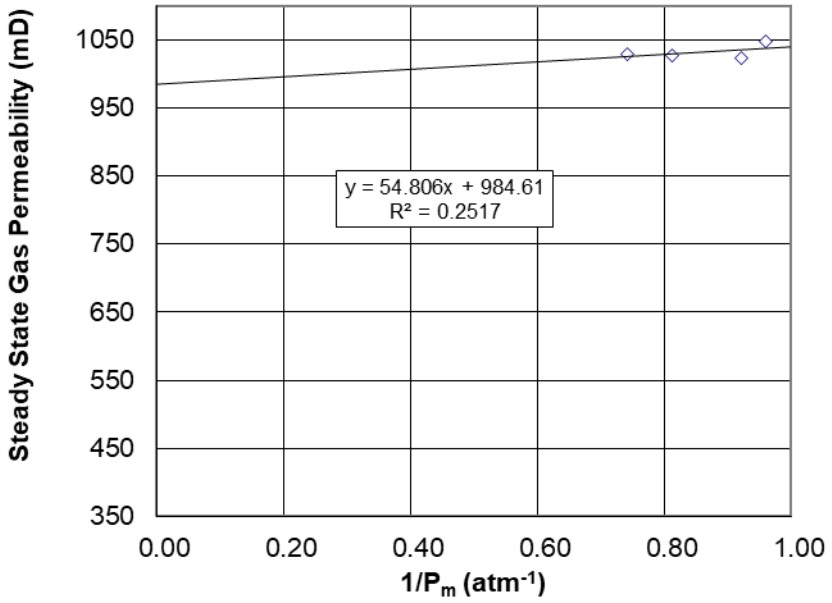

A-1: Klinkenberg corrected permeability for SP 1

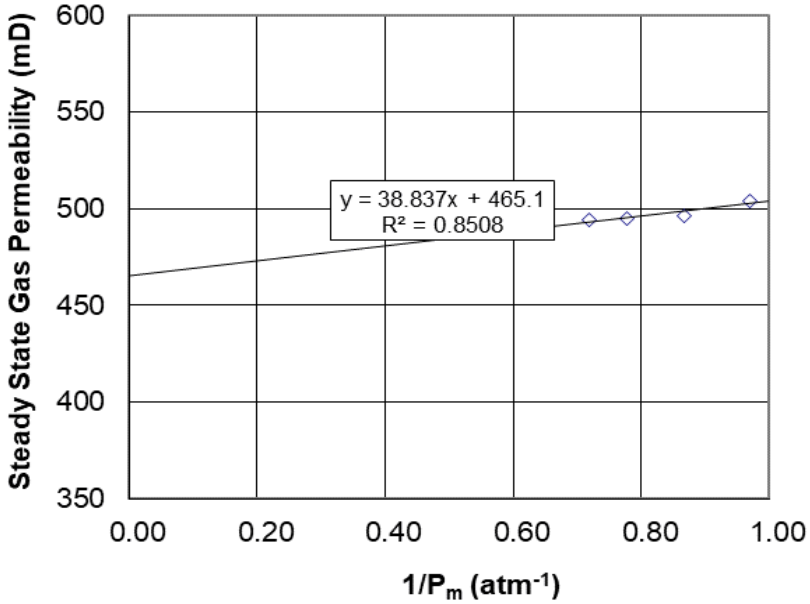

A-2: Klinkenberg corrected permeability for SP 3

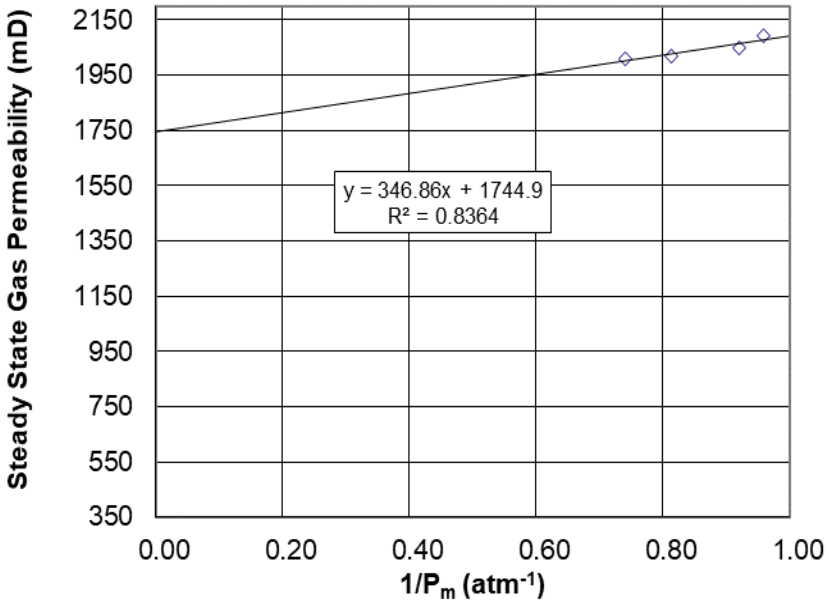

A-3: Klinkenberg corrected permeability for SP 4

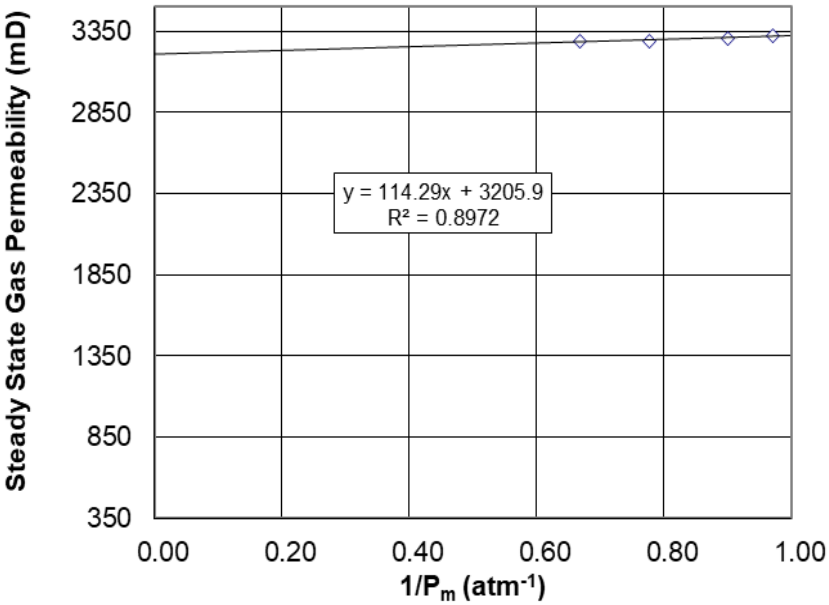

A-4: Klinkenberg-corrected permeability for SP 5

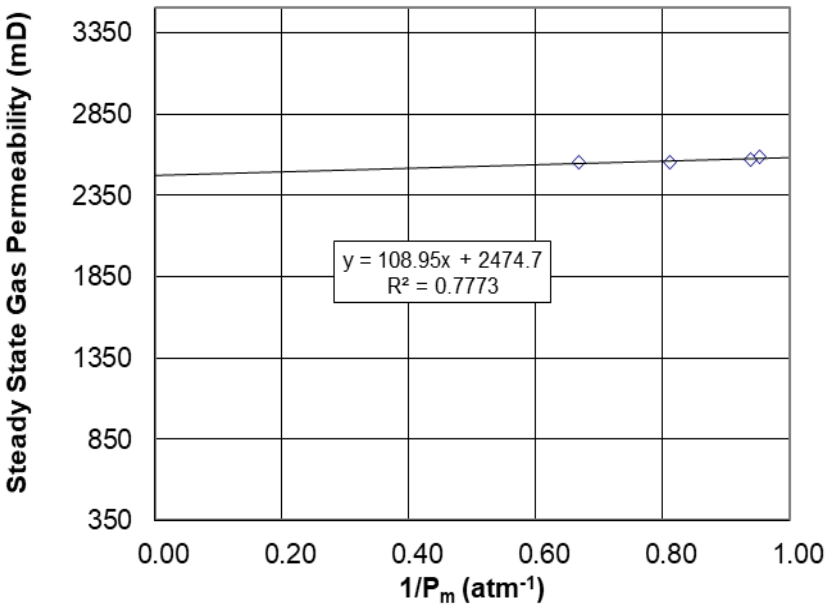

A-5: Klinkenberg corrected permeability for SP 6

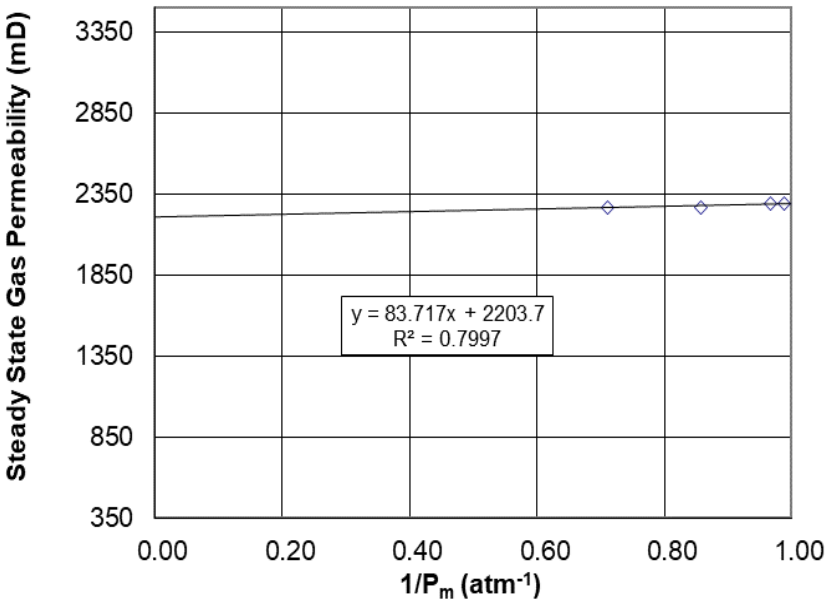

A-6: Klinkenberg corrected permeability for SP 7

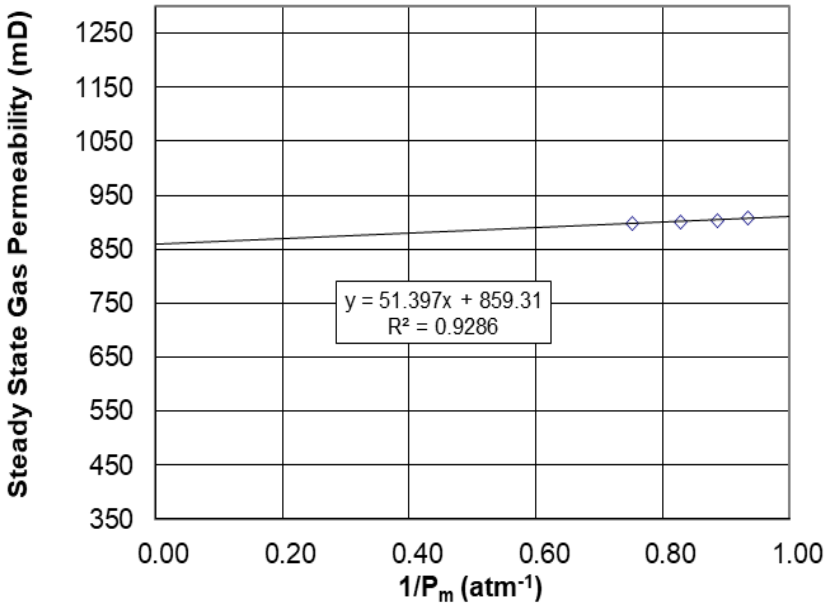

A-7: Klinkenberg corrected permeability for SP 8

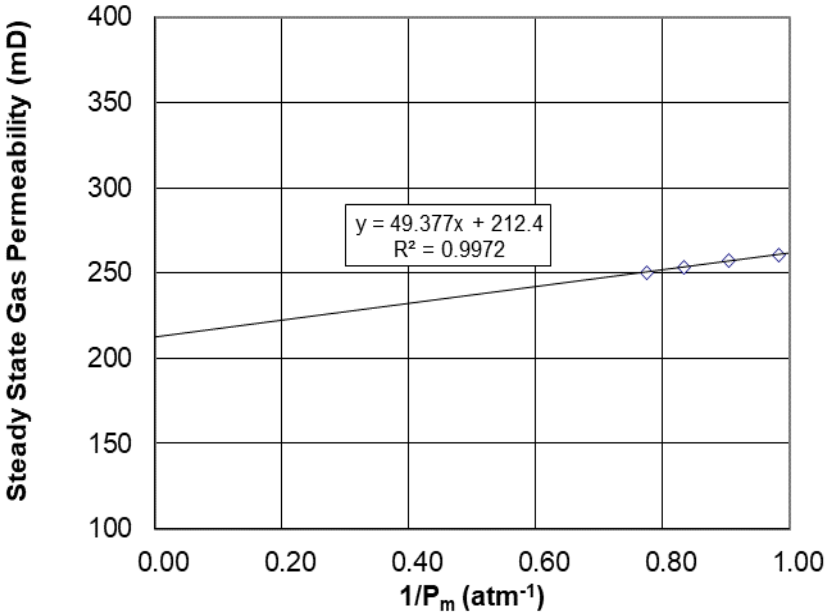

A-8: Klinkenberg corrected permeability for SP 10

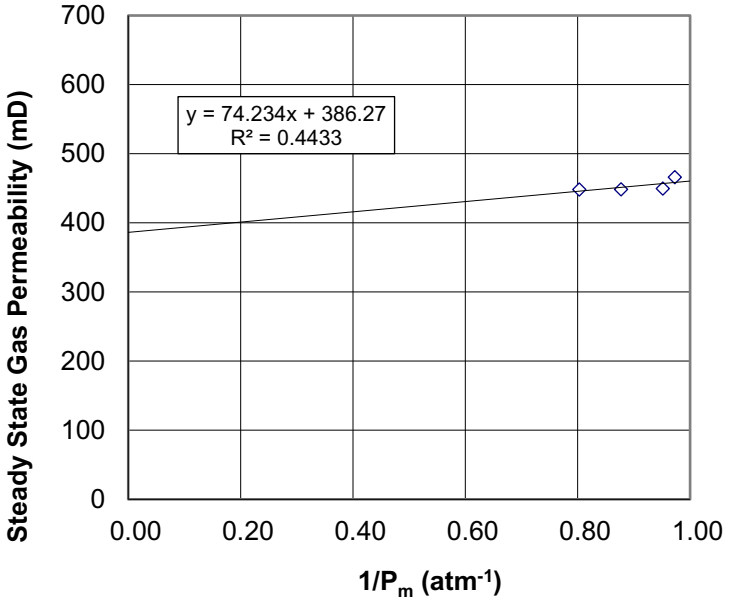

A-9: Klinkenberg-corrected permeability for SP 13

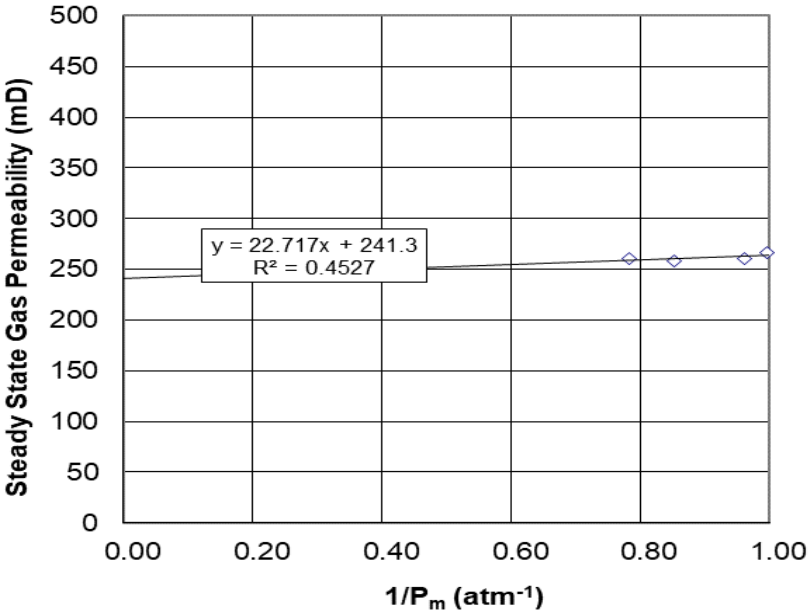

A-10: Klinkenberg corrected permeability for SP 17

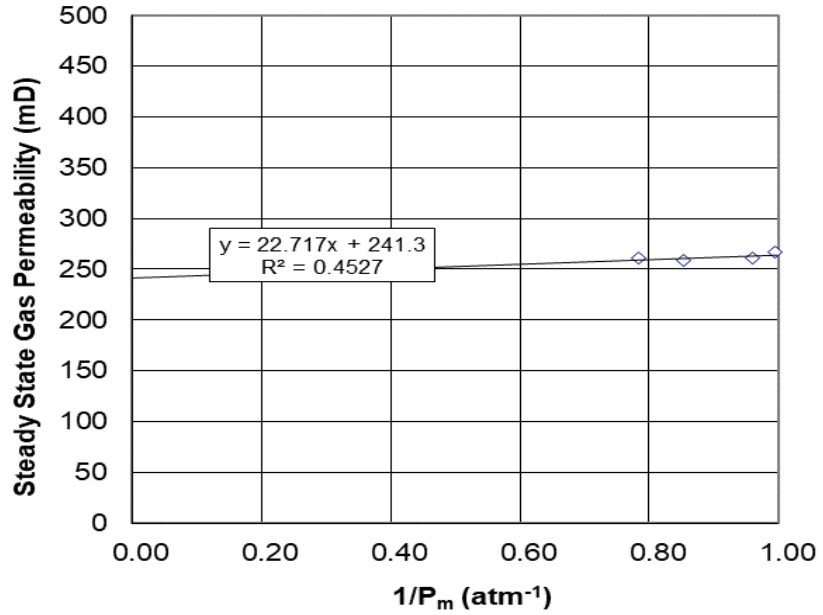

A-11: Klinkenberg corrected permeability for SP 17

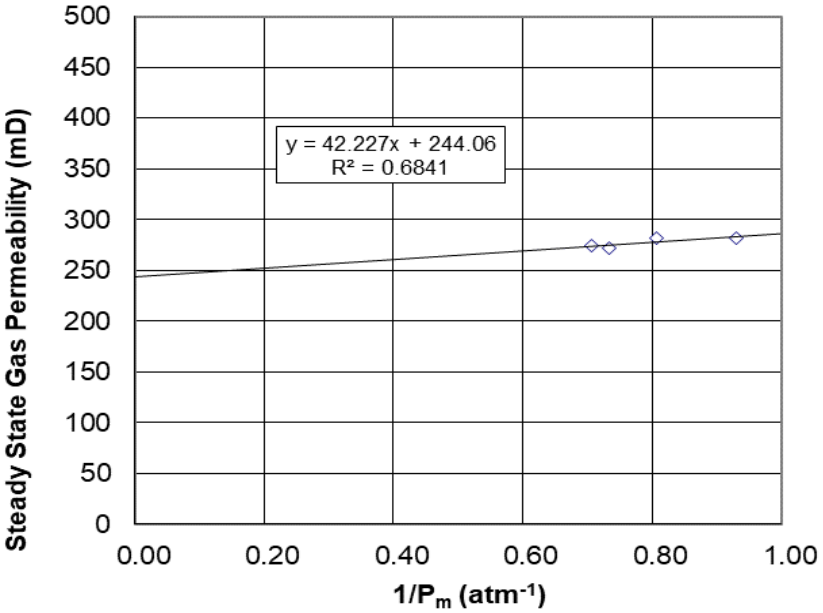

A-12: Klinkenberg corrected permeability for SP 17 Repeat 1

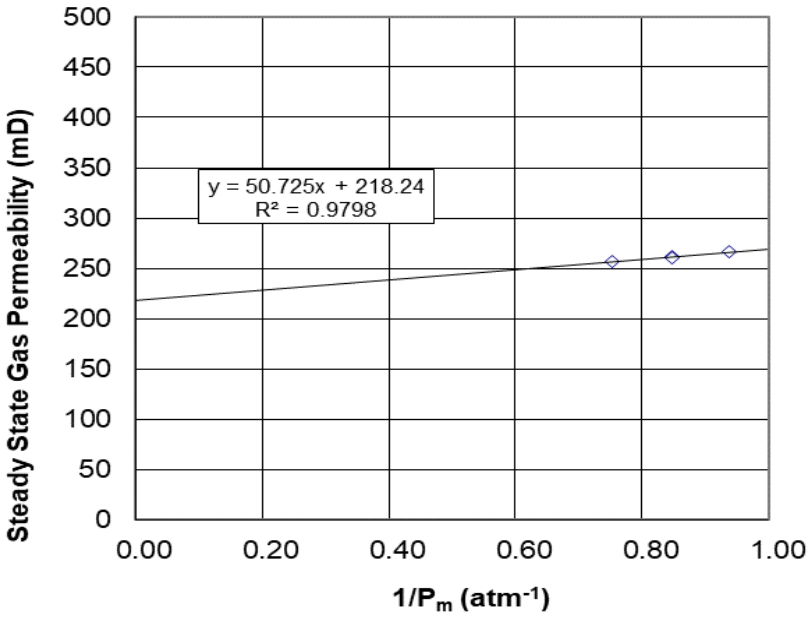

A -13: Klinkenberg corrected permeability for SP 17 Repeat 2

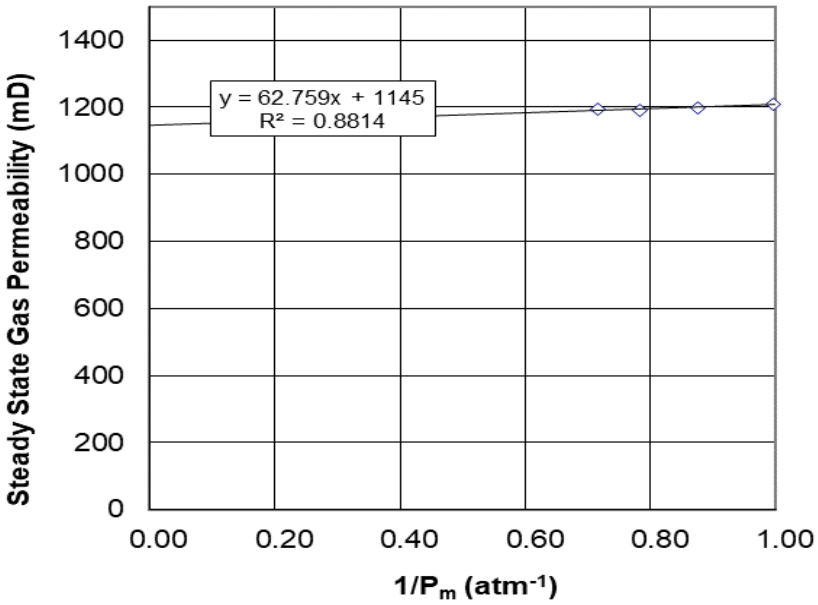

A-14: Klinkenberg corrected permeability for SP 18

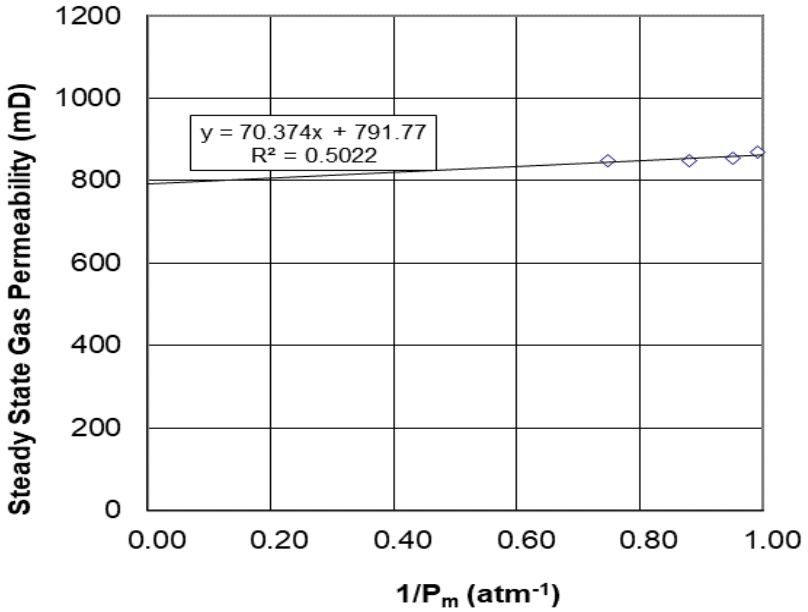

A-15: Klinkenberg corrected permeability for SP 19

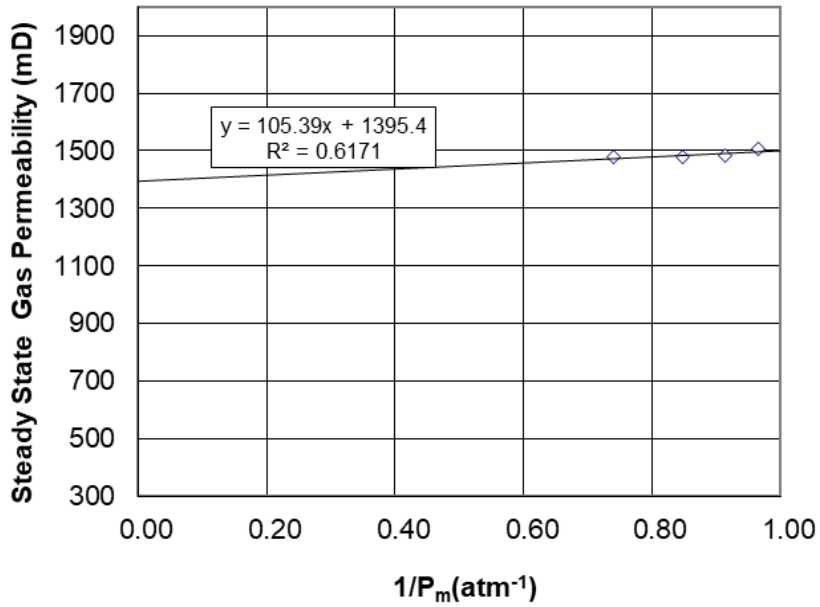

A-16: Klinkenberg corrected permeability for SP 20

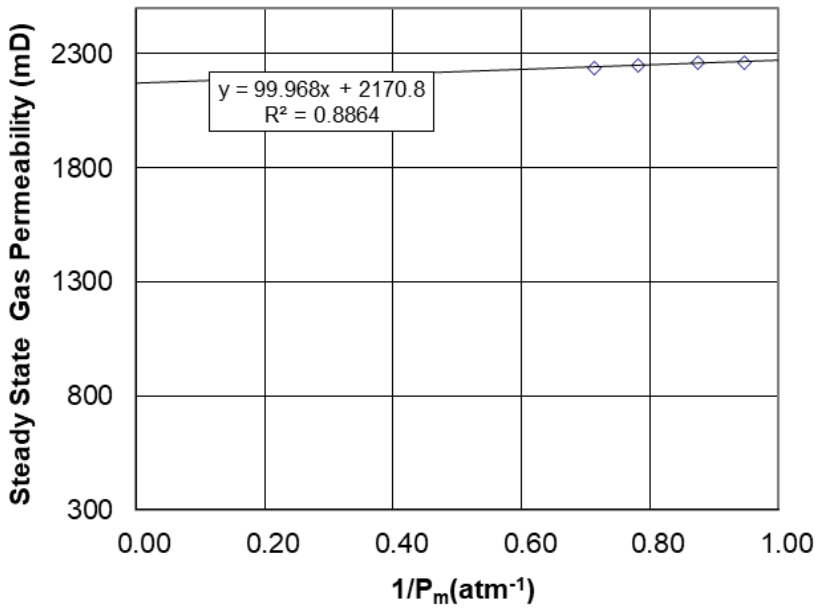

A -17: Klinkenberg corrected permeability for SP 22

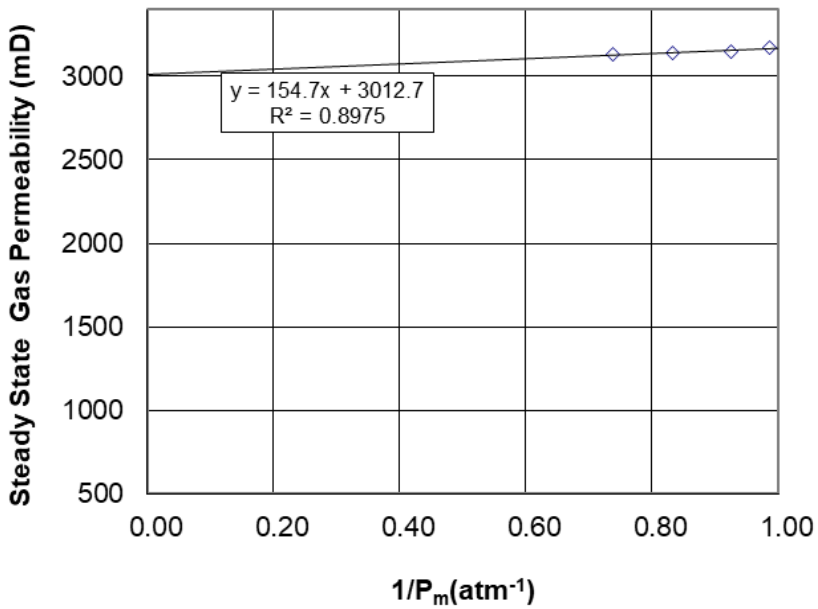

A-18: Klinkenberg corrected permeability for SP 23

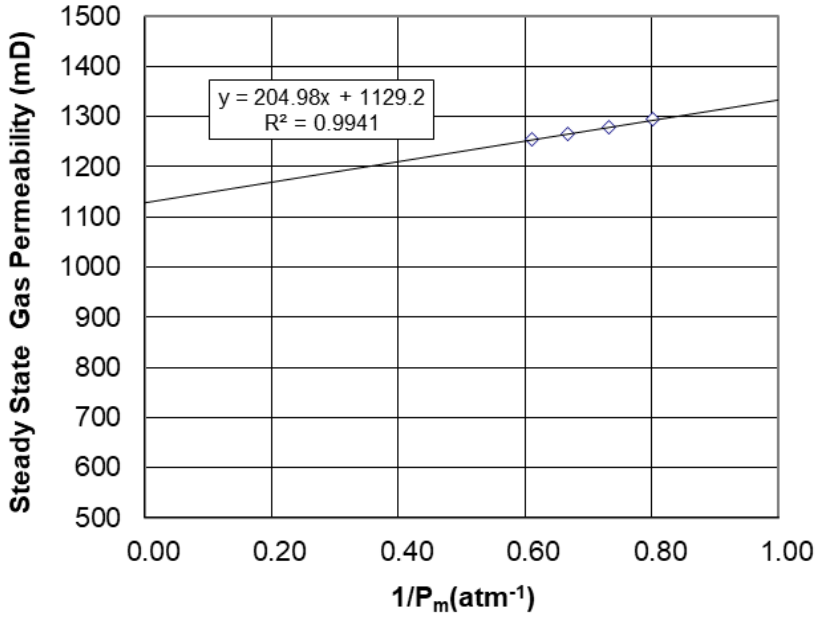

A-19: Klinkenberg corrected permeability for SP 30

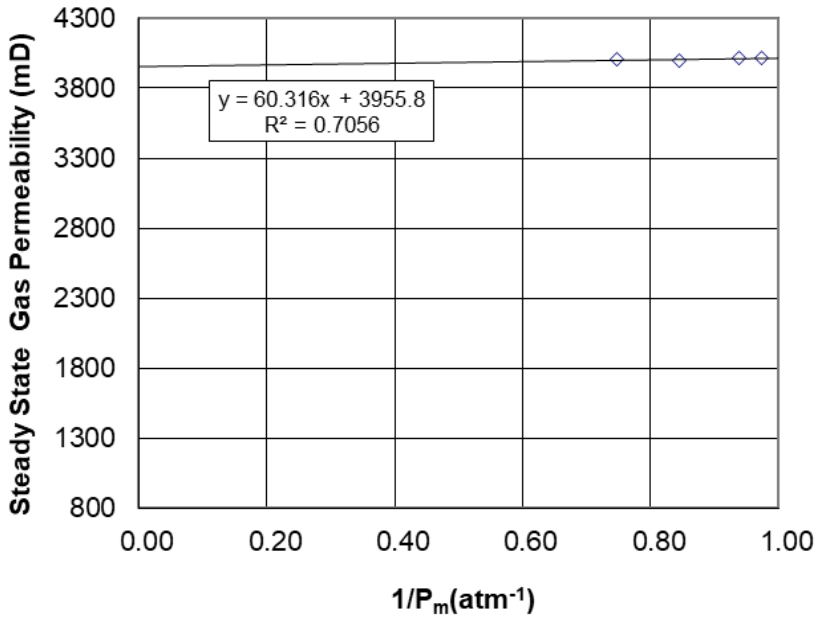

A-20: Klinkenberg corrected permeability for SP 31

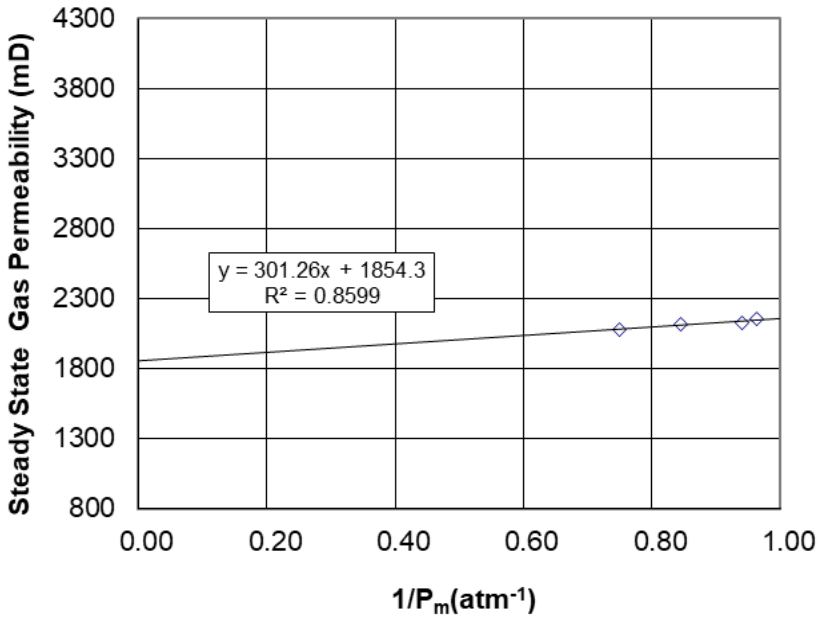

A -21: Klinkenberg corrected permeability for SP 32

Sample Name	Dia (mm)	Length (mm)	Atm. Press (psi)	Upstream P. (psig)	DP (psi)	Temp (°C)	Flow rate (cc/min)	K_g (mD)	$1/P_m$ (Abs Atm^{-1})	$(P_1)^2 - (P_2)^2$	Flow rate (cc/s)	Area (cm^2)
SP 1	35.0	40.1	14.7	0.620	0.026	20	15	1047.7	0.960	0.004	0.250	9.6
	35.0	40.1	14.7	1.330	0.128	20	73	1023.0	0.920	0.019	1.217	9.6
	35.0	40.1	14.7	3.610	0.456	20	259	1027.5	0.813	0.076	4.317	9.6
	35.0	40.1	14.7	5.500	0.727	20	411	1028.5	0.741	0.134	6.850	9.6
							kl =	984.6				
SP 3	34.5	43.0	14.7	0.500	0.102	20	26	504.3	0.970	0.014	0.433	9.3
	34.5	43.0	14.7	2.340	0.240	20	60	496.4	0.869	0.038	1.000	9.3
	34.5	43.0	14.7	4.380	0.370	20	92	495.1	0.778	0.065	1.533	9.3
	34.5	43.0	14.7	6.050	0.632	20	156	494.2	0.719	0.120	2.600	9.3
							kl =	465.1				
SP 4	35.0	47.0	14.7	0.180	0.010	21	10	2094.6	0.988	0.001	0.167	9.6
	35.0	47.0	14.7	0.780	0.080	21	78	2046.9	0.990	0.011	1.300	9.6
	35.0	47.0	14.7	2.300	0.150	21	144	2019.1	0.868	0.024	2.400	9.6
	35.0	47.0	14.7	5.523	0.260	21	248	2010.2	0.731	0.048	4.133	9.6
							kl =	1744.9				
SP 5	35.0	41.0	14.7	0.440	0.011	21	20	3322.4	0.971	0.002	0.333	9.6
	35.0	41.0	14.7	1.640	0.031	21	56	3302.9	0.900	0.005	0.933	9.6
	35.0	41.0	14.7	4.230	0.050	21	90	3292.3	0.777	0.009	1.500	9.6
	35.0	41.0	14.7	7.320	0.083	21	149	3285.3	0.669	0.017	2.483	9.6
							kl =	3205.9				
SP 6	35.0	44.0	14.7	0.723	0.014	20	19	2587.7	0.953	0.002	0.317	9.6
	35.0	44.0	14.7	0.970	0.068	20	89	2571.2	0.940	0.010	1.483	9.6
	35.0	44.0	14.7	3.450	0.110	20	143	2556.1	0.812	0.018	2.383	9.6
	35.0	44.0	14.7	7.430	0.210	20	272	2551.1	0.667	0.043	4.533	9.6
							kl =	2474.7				
SP 7	35.0	47.0	14.7	0.180	0.017	19	19	2287.8	0.988	0.002	0.317	9.6
	35.0	47.0	14.7	0.540	0.078	19	85	2287.7	0.967	0.011	1.417	9.6
	35.0	47.0	14.7	2.500	0.140	19	151	2267.7	0.858	0.022	2.517	9.6
	35.0	47.0	14.7	6.100	0.250	19	269	2266.7	0.711	0.048	4.483	9.6
							kl =	2203.7				
SP 8	35.0	45.0	14.7	1.090	0.153	20.1	69	908.5	0.935	0.022	1.150	9.6
	35.0	45.0	14.7	2.006	0.277	20.1	124	903.7	0.887	0.043	2.067	9.6
	35.0	45.0	14.7	3.254	0.405	20.1	180	901.2	0.828	0.067	3.000	9.6
	35.0	45.0	14.7	5.086	0.525	20.1	232	898.7	0.753	0.095	3.867	9.6
							kl =	859.3				
SP 10	36.0	37.0	14.7	0.310	0.120	20.3	20	260.7	0.983	0.017	0.333	10.2
	36.0	37.0	14.7	1.900	0.680	20.3	110	257.3	0.904	0.102	1.833	10.2
	36.0	37.0	14.7	3.550	1.240	20.3	195	253.6	0.834	0.202	3.250	10.2
	36.0	37.0	14.7	5.120	1.730	20.3	266	250.5	0.775	0.304	4.433	10.2
							Kl =	212.4				

Sample Name	Dia (mm)	Length (mm)	Atm. Press. (psi)	Upstream P. (psig)	DP (psid)	Temp. (°C)	Flow rate (cc/min)	K_q (mD)	$1/P_m$ (Abs Atm^{-1})	$(P_1)^2 - (P_2)^2$	Flow rate (cc/s)	Area (cm^2)

SP 13	35.0	44.0	14.7	0.467	0.114	20.9	27	466.0	0.973	0.016	0.450	9.6
	35.0	44.0	14.7	0.890	0.286	20.9	65	449.6	0.951	0.041	1.083	9.6
	35.0	44.0	14.7	2.410	0.705	20.9	158	448.6	0.877	0.109	2.633	9.6
	35.0	44.0	14.7	4.250	1.290	20.9	285	448.3	0.803	0.219	4.750	9.6
							kl =	386.3				
SP 14	35.0	45.0	14.7	0.109	0.136	20.7	18	266.4	0.995	0.019	0.300	9.6
	35.0	45.0	14.7	0.990	0.796	20.7	101	261.0	0.961	0.113	1.683	9.6
	35.0	45.0	14.7	2.998	0.956	20.7	120	258.6	0.853	0.152	2.000	9.6
	35.0	45.0	14.7	4.970	1.830	20.7	227	260.8	0.784	0.318	3.783	9.6
							kl =	241.3				
	35.2	48.2	14.7	1.554	0.441	20.11	57	278.1	0.917	0.065	0.950	9.7
	35.2	48.2	14.7	2.270	0.666	20.11	85	276.2	0.883	0.103	1.417	9.7
SP 17	35.2	48.2	14.7	3.293	0.926	20.11	116	273.0	0.838	0.150	1.933	9.7
	35.2	48.2	14.7	5.297	1.292	20.11	159	270.0	0.759	0.232	2.650	9.7
							kl =	214.3				
	35.2	48.2	14.7	1.214	0.236	20.1	29	282.2	0.930	0.035	0.519	9.7
	35.2	48.2	14.7	3.758	0.476	20.1	58	281.5	0.807	0.080	1.038	9.7
SP 17 Repeat 1	35.2	48.2	14.7	5.779	0.892	20.1	104	271.7	0.734	0.165	1.860	9.7
	35.2	48.2	14.7	6.600	1.019	20.1	120	274.9	0.707	0.196	2.147	9.7
							kl =	244.1				
	35.2	48.2	14.7	1.021	0.138	20.1	16	266.1	0.939	0.020	0.286	9.7
	35.2	48.2	14.7	2.920	0.522	20.1	59	261.5	0.847	0.084	1.055	9.7
SP 17 Repeat 2	35.2	48.2	14.7	3.048	0.806	20.1	90	260.4	0.847	0.129	1.610	9.7
	35.2	48.2	14.7	5.343	1.095	20.1	120	256.7	0.754	0.198	2.147	9.7
							kl =	218.2				
SP 18	36.0	42.0	14.7	0.048	0.094	20.4	64	1209.3	0.997	0.013	1.067	10.2
	36.0	42.0	14.7	2.135	0.123	20.4	83	1197.9	0.876	0.019	1.383	10.2
	36.0	42.0	14.7	4.174	0.176	20.4	118	1191.4	0.782	0.031	1.967	10.2
	36.0	42.0	14.7	6.000	0.365	20.4	244	1192.9	0.716	0.069	4.067	10.2
							kl =	1145.0				
SP 19	36.0	39.0	14.7	0.133	0.017	20.5	9	870.0	0.991	0.002	0.150	10.2
	36.0	39.0	14.7	0.800	0.083	20.5	43	853.1	0.951	0.012	0.717	10.2
	36.0	39.0	14.7	2.100	0.201	20.5	103	846.7	0.880	0.031	1.717	10.2
	36.0	39.0	14.7	5.200	0.480	20.5	245	848.5	0.748	0.087	4.083	10.2
							kl =	791.8				

Sample Name	Dia (mm)	Length (mm)	Atm. Press. (psi)	Upstream P. (psig)	DP (psid)	Temp (°C)	Flow rate (cc/min)	K_g (mD)	$1/P_m$ (Abs Atm^{-1})	$(P_1)^2 - (P_2)^2$	Flow rate (cc/s)	Area (cm^2)
SP 20	36	39	14.7	0.52	0.012	20.2	11	1506.1	0.966	0.002	0.183	10.2
	36	39	14.7	1.4	0.061	20.2	55	1483.6	0.915	0.009	0.917	10.2

	36	39	14.7	2.7	0.155	20.2	139	1479.4	0.848	0.025	2.317	10.2
	36	39	14.7	5.32	0.326	20.2	291	1478	0.74	0.06	4.85	10.2
							kl =	1395.4				
SP 22	35	43	14.7	0.823	0.016	20.4	19	2262	0.947	0.002	0.317	9.6
	35	43	14.7	2.135	0.07	20.4	83	2263.3	0.875	0.011	1.383	9.6
	35	43	14.7	4.174	0.103	20.4	120	2248.9	0.781	0.018	2	9.6
	35	43	14.7	6	0.17	20.4	198	2240.5	0.713	0.032	3.3	9.6
							kl =	2170.8				
SP 23	35	43	14.7	0.23	0.026	21.3	43	3171.1	0.985	0.004	0.717	9.6
	35	43	14.7	1.21	0.075	21.3	123	3149.2	0.926	0.011	2.05	9.6
	35	43	14.7	3.02	0.16	21.3	261	3139.2	0.833	0.026	4.35	9.6
	35	43	14.7	5.32	0.242	21.3	393	3130	0.739	0.045	6.55	9.6
							kl =	3012.7				
SP 30	36	43	14.7	3.65	0.028	20.4	20	1294.4	0.801	0.005	0.333	10.2
	36	43	14.7	5.408	0.061	20.4	43	1278.4	0.732	0.011	0.717	10.2
	36	43	14.7	7.32	0.099	20.4	69	1264.9	0.669	0.02	1.15	10.2
	36	43	14.7	9.43	0.12	20.4	83	1255.6	0.611	0.027	1.383	10.2
							kl =	1129.2				
SP 31	35	44	14.7	0.405	0.008	20.5	17	4016.2	0.973	0.001	0.283	9.6
	35	44	14.7	0.965	0.045	20.5	92	4013.5	0.939	0.007	1.533	9.6
	35	44	14.7	2.74	0.083	20.5	169	4000.9	0.845	0.013	2.817	9.6
	35	44	14.7	5.045	0.142	20.5	289	4004	0.747	0.026	4.817	9.6
							kl =	3955.8				
SP32	35	44	14.7	0.544	0.01	21.5	11	2157	0.964	0.001	0.183	9.6
	35	44	14.7	0.943	0.037	21.5	40	2121.7	0.941	0.005	0.667	9.6
	35	44	14.7	2.74	0.093	21.5	100	2113.5	0.845	0.015	1.667	9.6
	35	44	14.7	4.98	0.198	21.5	209	2079.7	0.751	0.036	3.483	9.6
							Kl =	1854.3				

Permeability Estimation Using Swanson Model

B.1- Sample Calculation for Swanson Model

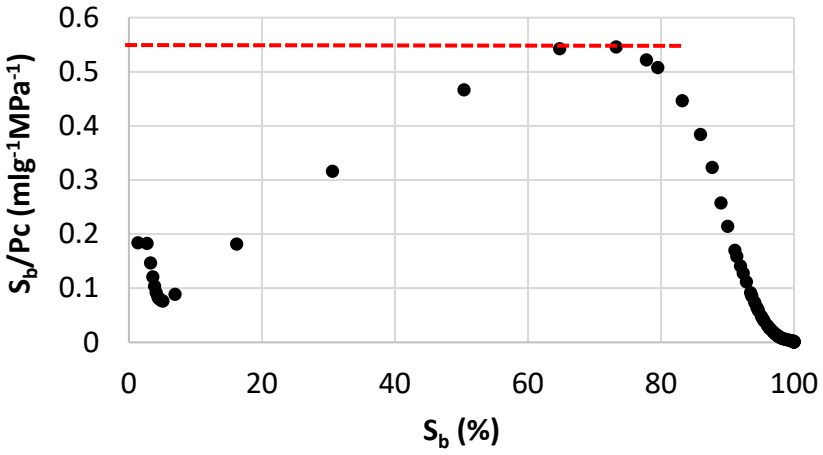

B-1: Graphs Showing the Swanson Parameter for SP 8

$k = a(S_b/P_c)^c_{max}$

a = 399 c = 1.691

K = 3.99*0.55^1.691

K = 145 mD

B.2- Determination of Swanson Parameter

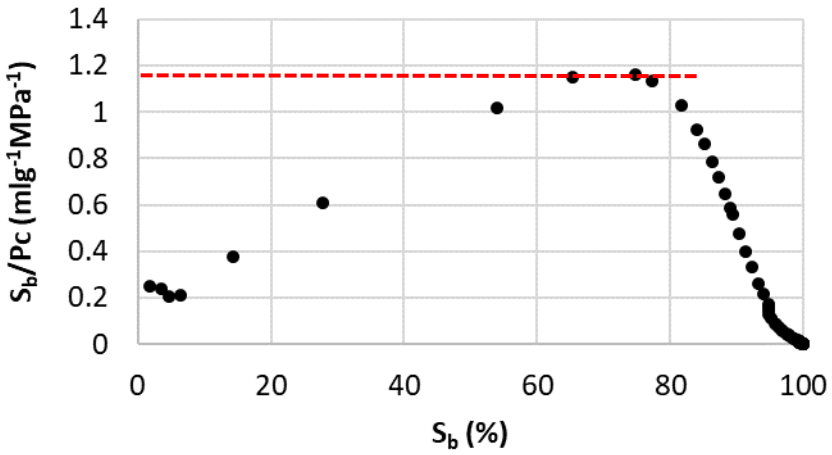

B-2: Swanson Parameter for SP 1

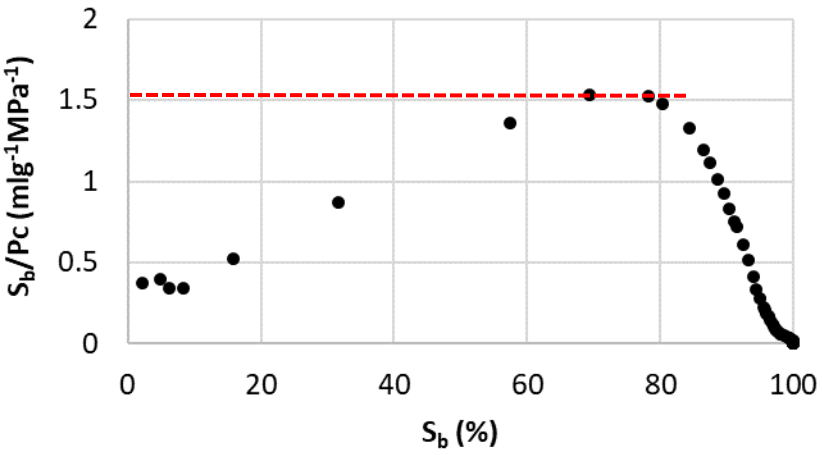

B-3: Swanson Parameter for SP 3

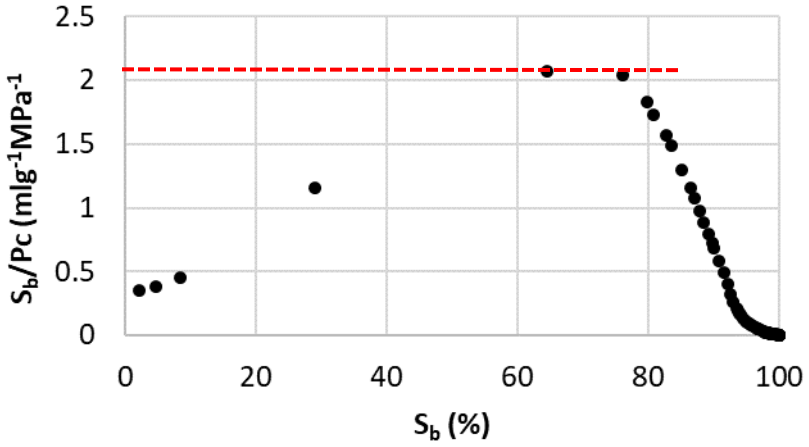

B-4: Swanson Parameter for SP 4

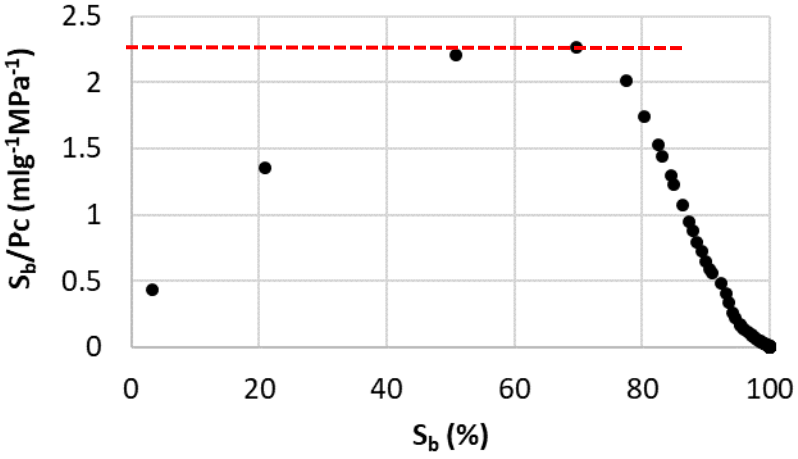

B-5: Swanson Parameter for SP 5

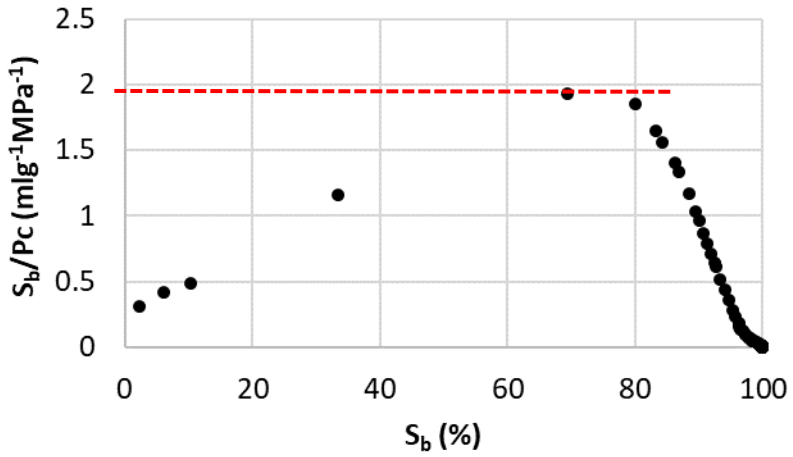

B-6: Swanson Parameter for SP 6

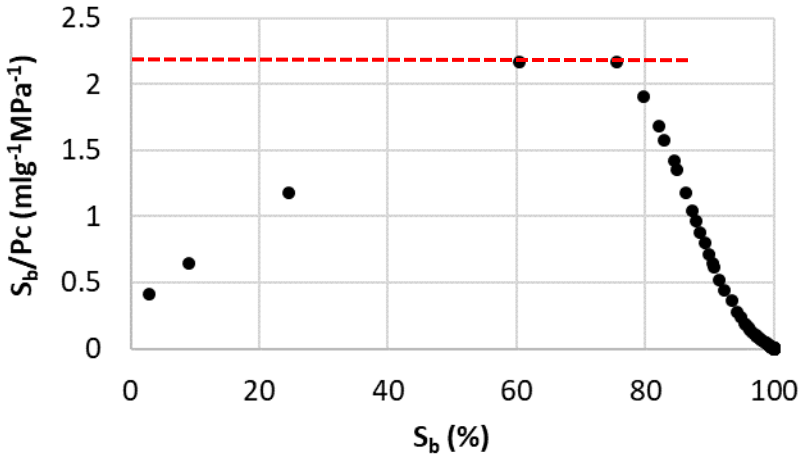

B-7: Swanson Parameter for SP 7

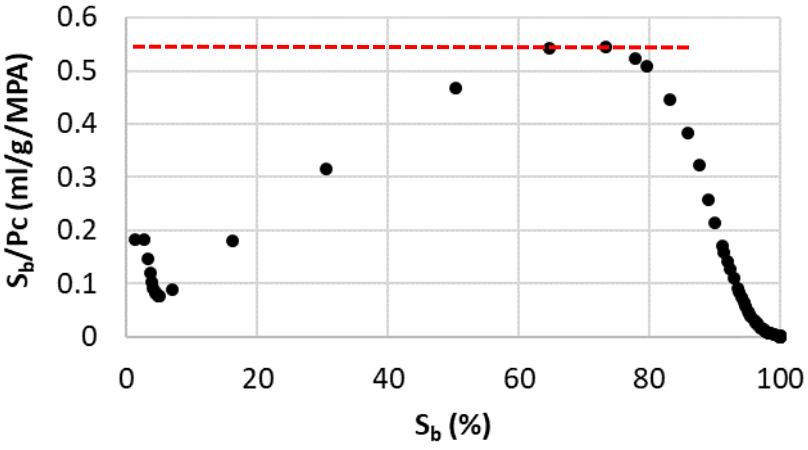

B-8: Swanson Parameter for SP 8

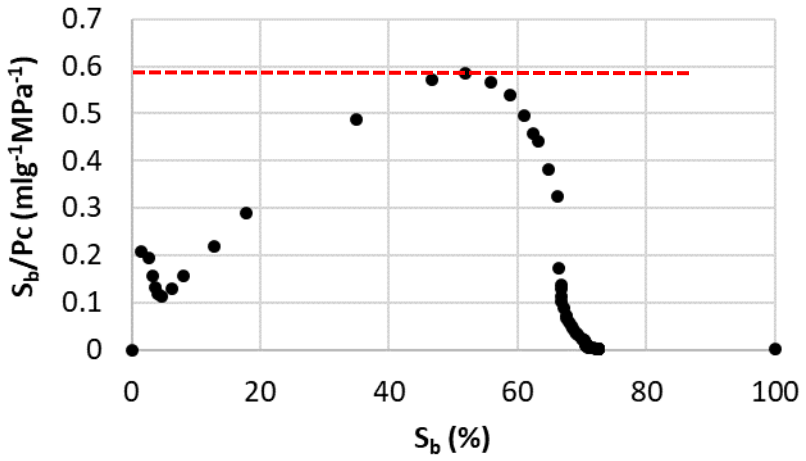

B-9: Swanson Parameter for SP10

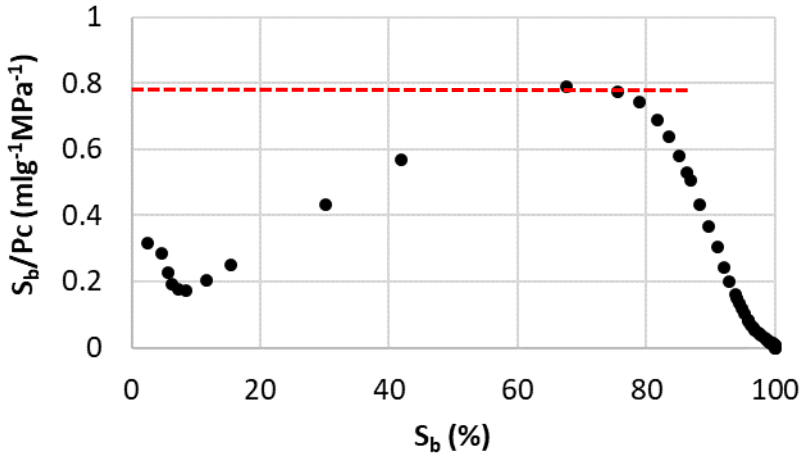

B-10: Swanson Parameter for SP 13

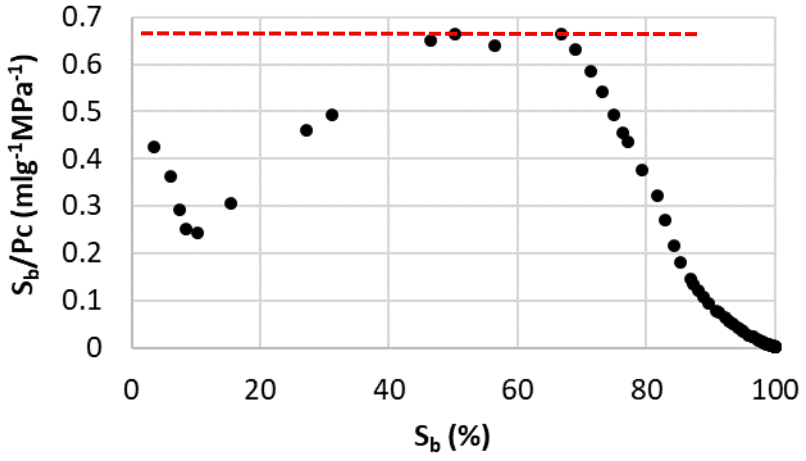

B-11: Swanson Parameter for SP 14

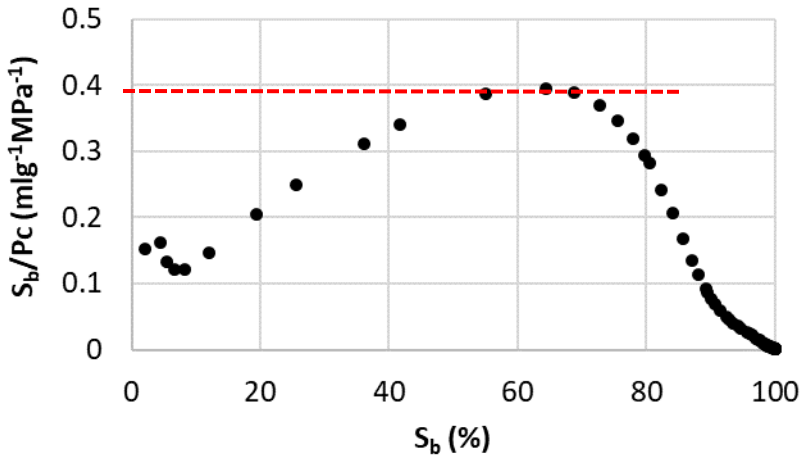

B-12: Swanson Parameter for SP 16

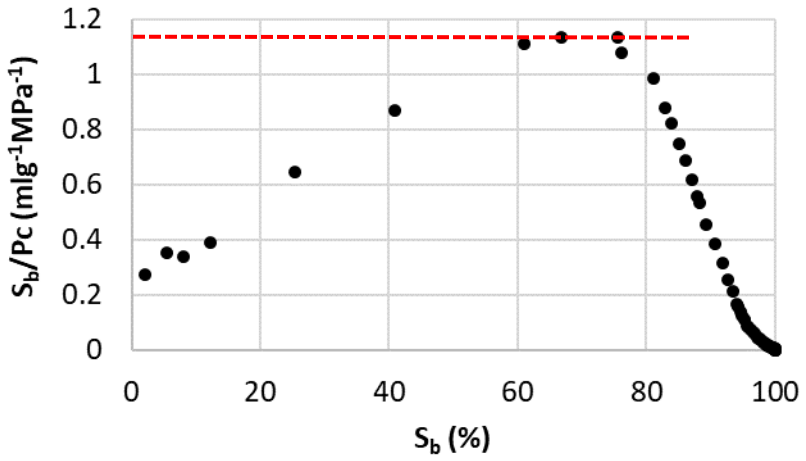

B-13: Swanson Parameter for SP 17

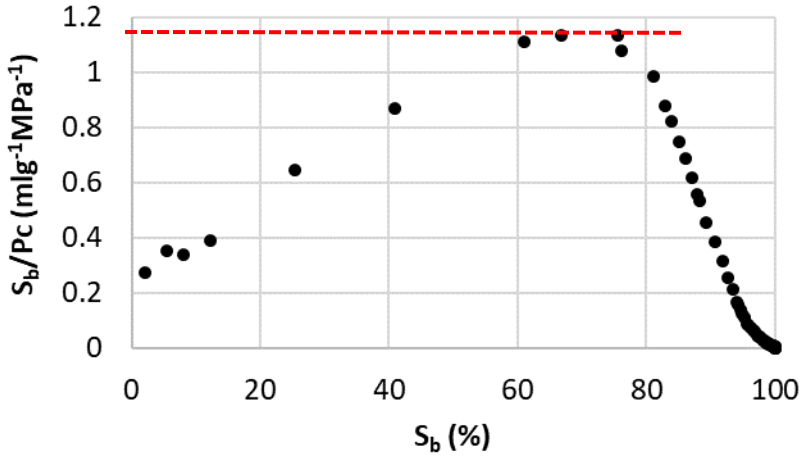

B-14: Swanson Parameter for SP 18

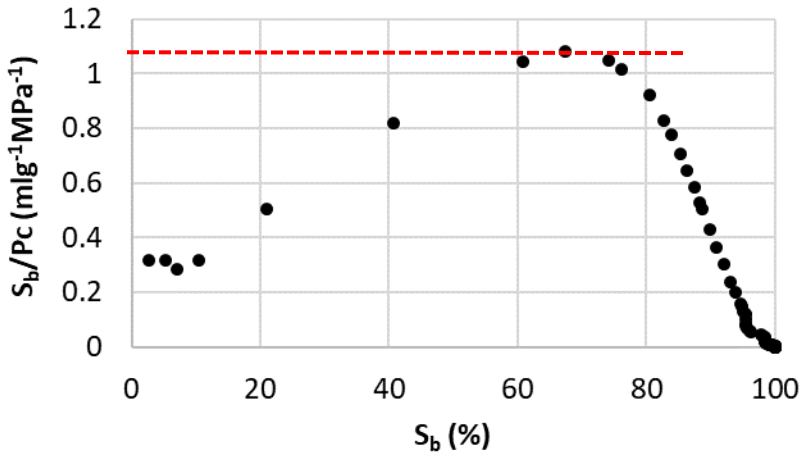

B-15: Swanson Parameter for SP 19

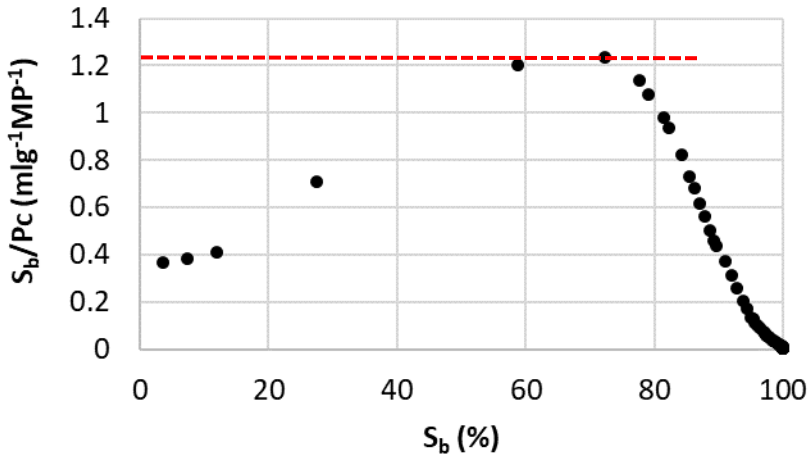

B-16: Swanson Parameter for SP 20

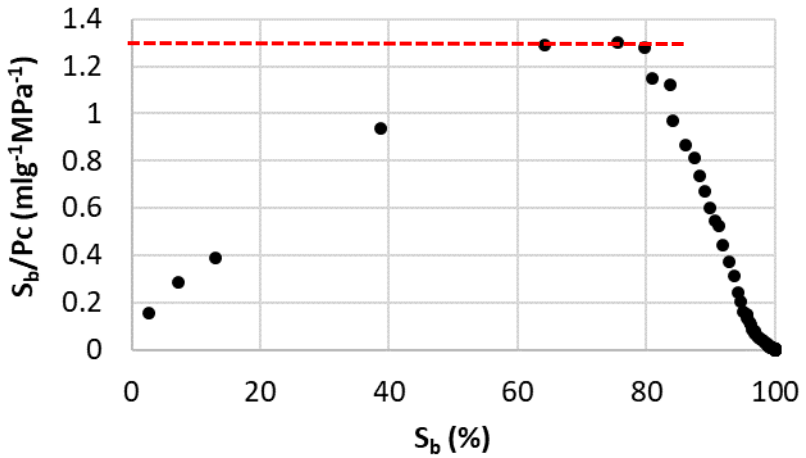

B-16: Swanson Parameter for SP 22

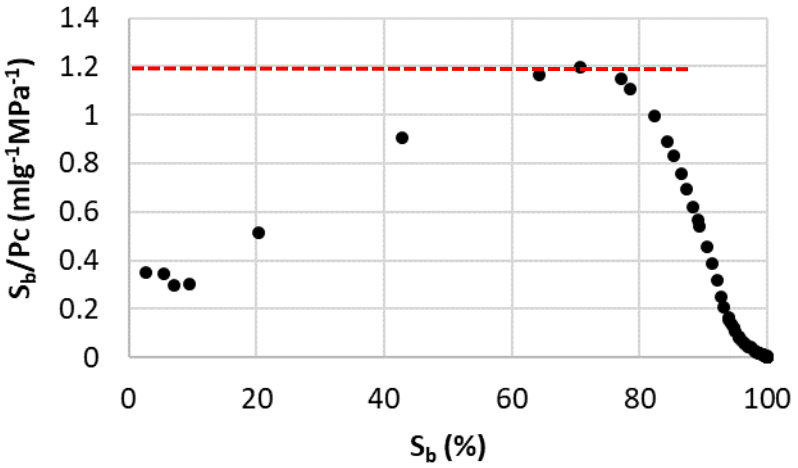

B-17: Swanson Parameter for SP 23

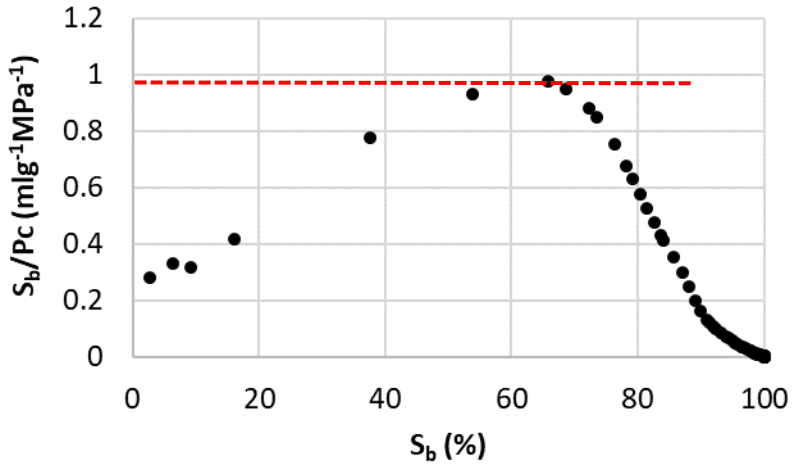

B-18: Swanson Parameter for SP 30

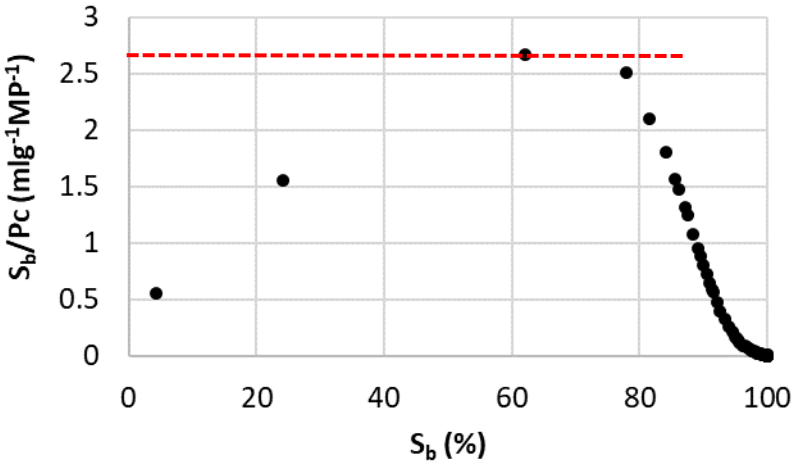

B-19: Swanson Parameter for SP 31

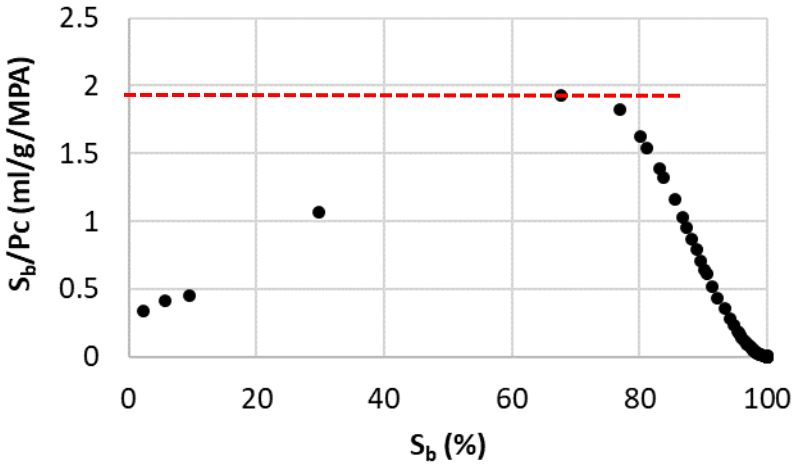

B-20: Swanson Parameter for SP 3

Sample ID	Depth (m)	Permeability measured by MIP	Permeability measured by Gas Permeametry	Porosity measured by MIP	Porosity measured by Helium pycnometry (Core Laboratories, 1999)
SP 1	3959.40 - 3959.79	652.0	984.6	19.2	18.8
SP 3	3961.85 - 3962.32	658.2	465.1	20.6	21.6
SP 4	3967.28 - 39 67.98	1747.4	1744.9	22.0	7.4
SP 5	3970.33 - 3970.67	2451.2	3205.9	19.0	22.0
SP 6	3970.96 - 3971.20	1704.5	2474.7	20.3	21.3
SP 7	3973.29 - 3973.58	20725	2203.7	20.5	21.9
SP 8	3978.57 - 3979.29	495.1	859.3	17.9	20.5
SP 10	4009.40 - 4009.60	181.2	212.4	14.3	16.1
SP 13	4017.54 - 4017.80	353.9	386.3	18.3	24.6
SP 14	4020.98 - 4021.28	359.2	241.3	17.6	19.1
SP 17	4027.94 - 4028.17	154.3	225.5	11.4	12.2
SP 18	4035.83 - 4036.08	753.9	1145	18.1	19.7
SP 19	4037.15 - 4037.49	618.7	791.8	17.9	20.2
SP 20	4040.31 - 4040.52	1207.5	1395.4	17.9	19.0
SP 22	4043.20 - 4043.39	1212.2	2170.8	18.0	19.5
SP 23	4045.73 - 4046.05	2867.7	3012.7	20.0	21.6
SP 30	4082.12 - 4082.34	605.1	1129.2	15.7	17.9
SP 31	4083.86 - 4084.10	3953.6	3955.8	18.8	21.0
SP 32	4088.01 - 4088.37	1669.1	1854.3	20.5	20.3